Applicability of the Acoustic Nonlinear Parameter 'β' for the Characterization of High Temperature Nickel-Based Superalloy Components

A Thesis

Submitted to

the School of Engineering of the

UNIVERSITY OF DAYTON

In Partial Fulfillment of The Requirements for

The Degree

Master of Science in Materials Engineering

by

Shaun L. Freed

UNIVERSITY OF DAYTON

Dayton, Ohio

August 2005

Applicability of the Acoustic Nonlinear Parameter 'β' for the Characterization of High Temperature Nickel-Based Superalloy Components

APPROVED BY:

Noel E. Ashbaugh, Ph.D.
Adviser Committee Chairman
Distinguished Research Engineer,
UDRI

Shamachary Sathish, Ph.D.
Committee Member
Graduate Faculty, Materials
Engineering Department

Daniel Eylon, Ph.D.
Committee Member
Professor & Program Director,
Materials Engineering Department

Andrew Rosenberger, Ph.D.
Committee Member
Senior Materials Research Engineer,
AFRL

Donald L. Moon, Ph.D.
Associate Dean, Graduate Engineering
Programs and Research
School of Engineering

Joseph E. Saliba, Ph.D., P.E.
Dean, School of Engineering

ABSTRACT

Fracture critical turbine engine components in USAF systems are managed according to the Engine Structural Integrity Program (ENSIP) guidance wherein disks are retired after usage when one in one thousand is predicted to contain a crack. The acoustic nonlinearity parameter (β) is reported to be a quantitative measurement of fatigue life consumption for a variety of materials. The goal of this research was to determine whether β can be used to measure the consumed fatigue life of turbine disks to cull the high usage disks from the USAF inventory and safely return to service components with lesser usage. While a thorough background is provided for understanding and acquiring β measurements through capacitive detection, the scientific contribution here is purely experimental. Previous β research, applied to fatigued Waspaloy specimens, was continued to investigate further β behavior throughout specimen life . β measurements were also obtained for a series of samples cut from used IN-100 first stage turbine engine disks. Results have shown, that while β measurements may not be as helpful as originally hoped in regards to characterizing remaining life for nickel-based superalloy components, potential does exist for application of β toward evaluating material processing and surface conditions.

ACKNOWLEDGMENTS

I would like to express my deepest gratitude to Dr. Noel Ashbaugh, for guiding this research, carefully advising and editing my thesis, and for providing me with this research opportunity.

This project was supported by the Air Force Research Laboratory, Materials and Manufacturing Directorate, of Wright Patterson AFB, in Dayton, Ohio through a contract with the University of Dayton Research Institute (DoD contract FA8650-04-C-5200 AFRL/MLLMN). It was a great honor to use AFRL's vast resources and to work with such knowledgeable people. I want to give a special thanks to Drs. Shamachary Sathish, Andrew Rosenberger, and Daniel Eylon for all their help and advice throughout this process.

I also want to thank Eric Burke of UDRI for training me in nonlinear acoustic data collection, Mark Ruddell of UDRI for his significant contribution to the understanding and setup of necessary electronic equipment, Phil Blosser of UDRI for conducting the fatigue loading of Waspaloy specimens, and Rick Reibel of UDRI for taking all the needed X-ray diffraction measurements.

Lastly, I would like to express great appreciation to my wife Joy for patiently enduring and supporting this effort in so many ways.

TABLE OF CONTENTS

LIST OF FIGURES

LIST OF TABLES

CHAPTER 1

INTRODUCTION

The acoustic behavior of solid materials has been studied through much of this century and a fairly thorough understanding of the physics has been developed. Many easily measured quantities can be determined by passing ultrasonic signals through a material such as wave velocity, attenuation, and displacement amplitude. The linear theory of acoustics predicts that if a signal of a given frequency is propagated through a medium, it will perfectly maintain that frequency and wave shape until final dissipation. In reality, an ultrasonic wave distorts in shape and generates harmonic frequencies (multiples of the initial frequency) as it propagates [1]. Nonlinear acoustics is the science of characterizing this behavior. The more "nonlinear" the material, the more distortion of the wave and generation of harmonic signals.

Of particular interest to this study is the non-dimensional parameter beta (β). Simply put, β is a first order measure of the nonlinearity of a material. Specifically, β is proportional to the ratio of the second harmonic amplitude to the fundamental amplitude squared:

$$\beta \propto \frac{A_2}{{A_1}^2} \quad . \tag{1.1}$$

The displacement amplitude of the longitudinal wave propagating at the input frequency is denoted as A_1 and is termed the fundamental signal. A_2 is the displacement

amplitude of the generated wave with twice the fundamental frequency and is called the second harmonic signal.

A number of material characteristics contribute to nonlinearity and subsequently to the β parameter. All materials have some inherent nonlinearity, but defects such as dislocations, cracks, and internal stresses may also contribute to the nonlinearity. Therefore, the β parameter could possibly be used to quantify and detect deviations within a material if one can accurately define all the acoustical nonlinearity contributions. β measurements could be a powerful tool in the field of nondestructive evaluation of materials.

In the field of aerospace, the ability to predict the life of mission critical components is important to achieve maximum use without compromising safety. Within the "Mechanical Behavior & Life Prediction" group of AFRL/ML, one goal is to characterize the life of engine disks which experience fatigue loading at high oxidizing temperatures. Currently, the service life of a disk is limited far shorter than most failures mandate, but precautionary measures are needed to protect from statistical rarities. Additionally, inspection intervals are established based on the time it takes for a crack to grow from an undetectable size to failure of the part. The goal of this research is to explore the possibilities of using the β parameter as a measure of crack precursor damage or of fatigue damage in general for a nickel-based superalloy engine disk. A measurement quantification of pre-crack damage would allow for more accurate calibration of life prediction methodologies and could provide for significant changes to the current turbine engine life management procedures.

CHAPTER 2

NONLINEAR ACOUSTIC THEORY & CALCULATIONS

2.1 Nonlinearity Parameter β

The parameter β, as applied to solid materials through the pioneering of Breazeale [2], is defined as the coefficient of the first order nonlinear term of the wave equation:

$$\frac{\partial^2 u}{\partial t^2} = v^2 \frac{\partial^2 u}{\partial z^2}(1 - \beta \frac{\partial u}{\partial z}) \quad , \tag{2.1}$$

where u is particle displacement parallel to the direction, z, of wave propagation, t is time, and v is the wave velocity. For a given frequency (f) and path length (l), an approximate solution to the wave equation can be given in the following form:

$$u = A_1 \sin(\omega t - kl) + \frac{\beta {A_1}^2 k^2 l}{8} \cos 2(\omega t - kl) \quad , \tag{2.2}$$

where

$$\begin{aligned} \omega &= 2\pi f, \\ k &= \frac{\omega}{v} = \frac{2\pi}{\lambda} = \text{wave number}, \\ \text{and } \lambda &= \text{wave length.} \end{aligned}$$

The coefficient of the second term can be assumed equal to the amplitude of the second harmonic signal A_2. Equation 2.2 allows for β to be defined in terms of the

fundamental and second harmonic amplitudes:

$$\beta = \frac{8}{k^2 l}\left(\frac{A_2}{{A_1}^2}\right) \quad . \tag{2.3}$$

According to this definition, all that is needed to determine β are the amplitude measurements of A_1 and A_2 along with the wave number and propagation length. The difficulty lies in the fact that the generated second harmonic displacement amplitudes are very small,on the order of 10^{-12}m - 10^{15}m. The three established techniques for measuring surface displacements of this magnitude are laser interferometry, contact transducers, and capacitive detection. Capacitive detection is the standard technique and the one chosen for this research. The theory of this technique is presented in Section 2.4, while the experimental procedure is explained in Chapter 3.

2.2 Corrections to β

An idealization that was used in deriving Equation 2.3 for β, is that the ultrasonic longitudinal wave propagates without losses. Ideally A_1 maintains its amplitude, A_2 continually grows in amplitude as more harmonic generation is added with path length, and both signals propagate along a straight path in a uniformly planer shape. This idealization is sometimes good enough for calculating β, but often times it is necessary to correct for both attenuation and diffraction. Fortunately, these phenomena are fairly well understood and quantified in past literature.

2.2.1 Attenuation

For this study, attenuation is considered to be any effect that causes losses to wave amplitudes through energy absorption. When testing materials with minimal attenuation, such as aluminum, or thin samples with a short propagation length,

attenuation effects to β can be neglected. Otherwise a correction factor is developed [3, 4, 5].

Attenuation of any wave is characterized by an exponential decay in amplitude versus propagation length:

$$A = A_0 e^{-\alpha z} \quad . \tag{2.4}$$

An attenuated wave has an initial amplitude A_0 at a given point and then, after traveling a distance z, has a decreased amplitude of A. The measure of attenuation is characterized by the coefficient α.

To begin the development of an attenuation correction factor we must first assume that A_1 losses due to harmonic generation are minimal in comparison to attenuation losses and therefore can be neglected. Secondly, however, we assume that the magnitude of A_2 can be characterized as the sum effect of continual amplitude generation from A_1 minus the attenuation of A_2. Therefore, the change in A_2 with respect to z is determined by superposition of the following two derivatives:

- Change due to attenuation:

$$\begin{aligned} A_2 &= A_{0_2} e^{-\alpha_2 z} \\ \frac{dA_2}{dz} &= -\alpha_2 A_{0_2} e^{-\alpha_2 z} \\ &= -\alpha_2 A_2 \end{aligned}$$

- Change due to harmonic generation (from Equation 2.3):

$$\begin{aligned} A_2 &= \frac{1}{8}\beta k^2 {A_1}^2 z \\ \frac{dA_2}{dz} &= \frac{1}{8}\beta k^2 {A_1}^2 \\ &= \frac{1}{8}\beta k^2 {A_{0_1}}^2 e^{-2\alpha_1 z} \end{aligned}$$

The resulting differential equation becomes:

$$\frac{dA_2}{dz} = \frac{1}{8}\beta k^2 A_{0_1}^2 e^{-2\alpha_1 z} - \alpha_2 A_2 \quad . \tag{2.5}$$

By rearranging Equation 2.5 into the form $\frac{dy}{dx} + P(x)y = Q(x)$, a standard solution is given in the following form:

$$ye^{\int P(x)dx} = \int Q(x)e^{\int P(x)dx}dx + C \quad . \tag{2.6}$$

Therefore, the solution goes as follows:

$$\underbrace{\frac{dA_2}{dz}}_{\frac{dy}{dx}} + \underbrace{\alpha_2 A_2}_{P(x)y} = \underbrace{\frac{1}{8}\beta k^2 A_{0_1}^2 e^{-2\alpha_1 z}}_{Q(x)} \tag{2.7}$$

From Equation (2.6):

$$\begin{aligned}
A_2 e^{\int \alpha_2 dz} &= \int (\frac{1}{8}\beta k^2 A_{0_1}^2 e^{-2\alpha_1 z} e^{\int \alpha_2 dz})dz + C \\
&\rightarrow \int \alpha_2 dz = \alpha_2 z \\
&\rightarrow \int (\frac{1}{8}\beta k^2 A_{0_1}^2 e^{-2\alpha_1 z} e^{\int \alpha_2 dz})dz \\
&= \frac{1}{8}\beta k^2 A_{0_1}^2 \int e^{(\alpha_2 - 2\alpha_1)z} dz \\
&= \frac{1}{8}\beta k^2 A_{0_1}^2 \left[\frac{e^{(\alpha_2 - 2\alpha_1)z}}{(\alpha_2 - 2\alpha_1)}\right] \\
A_2 e^{\alpha_2 z} &= \frac{1}{8}\beta k^2 A_{0_1}^2 \left[\frac{e^{(\alpha_2 - 2\alpha_1)z}}{(\alpha_2 - 2\alpha_1)}\right] + C \\
A_2 &= \frac{1}{8}\beta k^2 A_{0_1}^2 \left[\frac{e^{-2\alpha_1 z}}{(\alpha_2 - 2\alpha_1)}\right] + \frac{C}{e^{\alpha_2 z}}
\end{aligned}$$

For $z = 0, A_2 = 0$

$$C = -\frac{\beta k^2 A_{0_1}^2}{8(\alpha_2 - 2\alpha_1)}$$

The equation for A_2 then becomes:

$$A_2 = \frac{1}{8}\beta k^2 A_{0_1}^2 \left[\frac{e^{-2\alpha_1 z} - e^{-\alpha_2 z}}{(\alpha_2 - 2\alpha_1)}\right] \quad . \tag{2.8}$$

Including these corrections for attenuation and substituting in length l for z, the solution to the wave equation (Equation 2.1) for displacement becomes

$$u = A_{0_1} e^{-\alpha_1 l} \sin(\omega t - kl) + \frac{1}{8}\beta k^2 {A_{0_1}}^2 \left[\frac{e^{-2\alpha_1 l} - e^{-\alpha_2 l}}{(\alpha_2 - 2\alpha_1)}\right] \cos 2(\omega t - kl) \quad .$$

Since we want to measure A_1 and not A_{0_1}, we substitute in A_1 for $A_{0_1} e^{-\alpha_1 l}$:

$$u = A_1 \sin(\omega t - kl) + \frac{1}{8}\beta k^2 {A_1}^2 \left[\frac{1 - e^{(\alpha_1 - \alpha_2)l}}{(\alpha_2 - 2\alpha_1)}\right] \cos 2(\omega t - kl) \quad .$$

By comparing this equation with our previous one (Equation 2.2) and again setting the coefficient of the second term equal to A_2, we can now equate a new description for β in terms of our "raw" uncorrected β:

$$\beta = \beta_{raw} \left[\frac{(\alpha_2 - 2\alpha_1)l}{1 - e^{-(\alpha_2 - 2\alpha_1)l}}\right] \quad . \tag{2.9}$$

From Equation 2.9 we can see that the effect of attenuation is solely attributed to path length l and the difference in attenuation coefficients.

2.2.2 Diffraction

While attenuation is signal loss due to absorption, diffraction is considered to be the signal dilution due to the spreading out of the wave. Historically, many have not considered the effects of diffraction if large transducers and short path lengths are used. However, when attempting to compare samples of different geometry, or with different source radii, corrections are very important. Diffraction corrections for a wave introduced by a single source have been long developed and agreed upon. The difficulty here is that β depends on A_2 as well as A_1. While A_1 can be considered as resulting from a single source, A_2 is being continually generated. As a result, many different approaches have been suggested. Many of the different methods correspond to the radius differences of the send and receive transducers.

To keep things simple and consistent, this project has worked only with send and receive transducers of matching diameters. With this technique, only two different approaches have been used. Hurley [6] has developed a correction equation through an analytical approach. Blackburn and Breazeale [7] used a quite different approach that was developed experimentally. The two approaches are compared in reference [3] where noticeable differences in β are demonstrated, depending on which method is used. Since the latter approach proved to be a more consistent correction for the experimental results, it is used exclusively in this research.

A diffraction correction factor for the amplitude of a single wave is merely a function of path length z, wave length λ, and source radius r. It is derived by solving the Lommel diffraction correction integral, which has been accomplished through numerous numerical and direct methods [8, 9, 10, 11]. Rogers and Vanburen [11] derived a closed form expression for the Lommel diffraction correction D_L in the following form:

$$D_L = \left[\cos(\frac{2\pi}{s}) - J_0(\frac{2\pi}{s})\right]^2 + \left[\sin(\frac{2\pi}{s}) - J_1(\frac{2\pi}{s})\right]^2 \quad , \tag{2.10}$$

where

$$s = \frac{l\lambda}{r^2} \quad = \quad \text{Seki parameter,}$$

$$\text{and } J_0, J_1 \quad = \quad \text{Bessel Functions.}$$

This approximation is valid for $(kr)^{1/2} \gg 1$.

Through experimental verification, Blackburn and Breazeale showed that the diffraction correction for β could be expressed as $D_\beta = (D_{L_{A_1}})^2$ [7]. The approach of Blackburn and Breazeale does not include any diffraction correction contribution from A_2.

2.2.3 Corrections Conclusions

The final equation to be used throughout this project is

$$\beta = \beta_{raw}(D_{L_{A_1}})^2\left[\frac{(\alpha_2 - 2\alpha_1)l}{1 - e^{-(\alpha_2 - 2\alpha_1)l}}\right] \quad . \tag{2.11}$$

It is important to remember that while β in theory is an absolute value for a given material sample, in practice no standard method of correction has been fully agreed upon among different research groups. Therefore, when comparing different research, the methods and variables being used must be defined.

Also of note: any reported β values from this project measured on samples with a thickness $\leq$ 4mm are β_{raw} values with no correction factors applied. This is due first of all to the assumption that attenuation and diffraction effects are minimal for short path lengths. Secondly, other complexities have been found to arise for thin samples that make absolute β measurements difficult. In such cases it is best to simply compare samples of the same thickness. Further discussion of such difficulties is given in the following chapters.

2.3 Influences of β

Many theoretical models have been developed to predict the behavior of β for a variety of metals [12, 13]. The lattice structure gives a material its base source for nonlinearity. Different material deviations consequently contribute to the total material nonlinearity. Dislocations, and specifically dislocation dipoles, are predicted by theory to have a considerable effect on β. Since dislocation dipoles are induced through cyclic fatigue, β becomes a theoretical indicator of fatigue life consumption. Internal stresses and cracks are also predicted contributors to β, but Cantrell [13]

reports that contributions from cracks in polycrystaline nickel are only significant upon reaching a fully macro size.

Many of these β contributions have been demonstrated experimentally as well. Cantrell and Yost report a monotonic increase of β for fatigued aluminum 2024-T4 [14]. Frouin correlates dislocation density with β for Ti-6Al-4V [5]. Research by Burke [15], preceding the current work, also reports a fatigue influence on β for Waspaloy. Effects of surface features present on used engine components such as shot peening, oxidation, and roughness on β measurements have not been fully explored.

2.4 Capacitive Gap Transducer for Displacement Measurement

The established standard method of signal reception for finite amplitude measurements is through a capacitive detector (Figure 2.1). What makes this type of transducer ideal for β measurements is that it's response is independent of frequency and is sensitive to extremely small displacements. A thorough description of the equipment will be discussed in Chapter 3, but the theory of operation is explained here.

The idea of a capacitive gap transducer is to create a parallel plate capacitor between the sample surface of interest and an electrode. Knowing the permittivity ε of the gap, the area a of the electrode, and the distance d between surfaces, the capacitance is calculated as [16]

$$C = \frac{a\varepsilon}{d} \quad . \tag{2.12}$$

As the surface vibrates, the capacitance varies inversely to the changing gap distance d. By placing a large bias voltage and in series resistance across the capacitive gap,

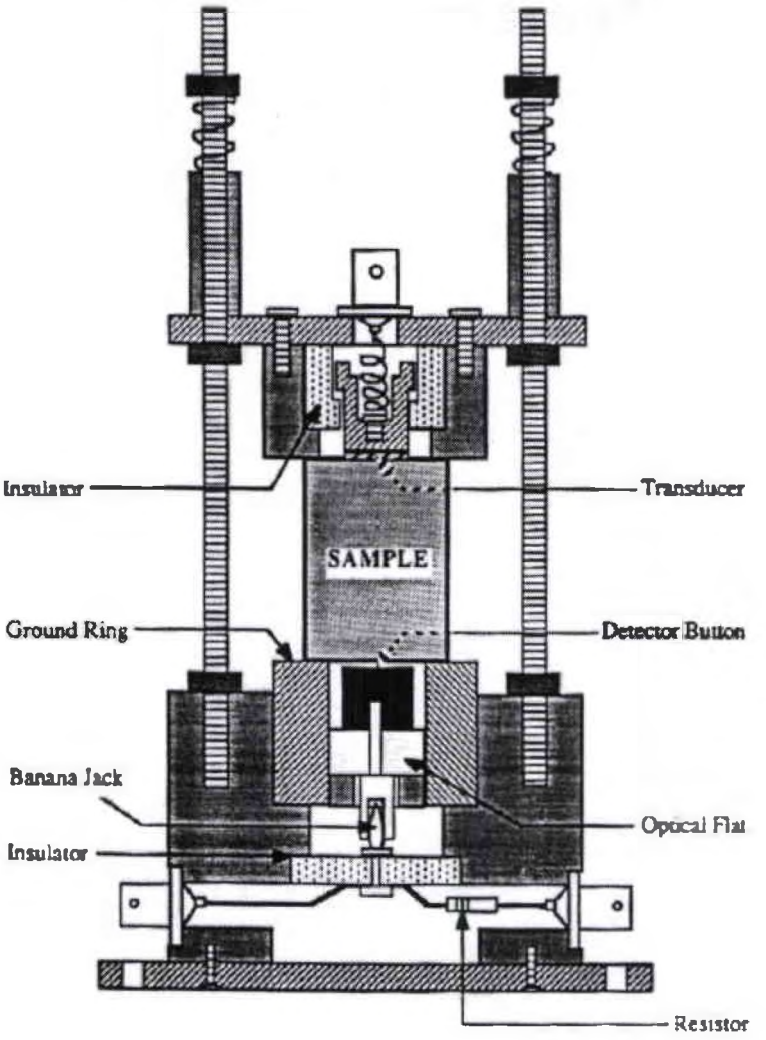

Figure 2.1: Diagram of Capacitive Detector [5]

a generated sinusoidally alternating voltage v_g can be detected. The voltage peak to peak amplitude V_g can then be converted into displacement amplitudes.

To better understand this, lets look at the voltage across a variable gap capacitor. For a capacitor, the voltage V is defined in terms of the charge Q built up on the opposing plates and the capacitance:

$$V = \frac{Q}{C} \quad . \tag{2.13}$$

The initial voltage V_0, once the capacitor is fully charged, across the static surfaces separated by a distance d_0, as shown in Figure 2.2, is equal to the bias voltage V_b applied. As one surface vibrates sinusoidally with a peak to peak amplitude of x, the gap distance varies between a minimum magnitude d_1 and maximum d_2. The capacitance changes instantaneously as the gap distance differs, but the rate that Q changes depends on the magnitude of the resistance R and the static capacitance C_0.

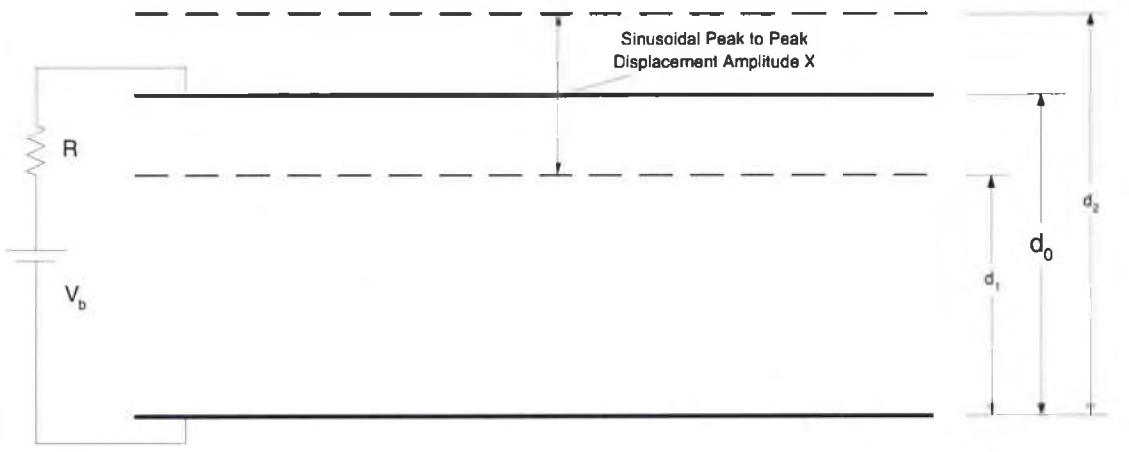

Figure 2.2: Variable Gap Parallel Plates of a Capacitor

For a simple R-C circuit, as shown in Figure 2.2, charge flows from a bias voltage source to charge up a capacitor as quantified by the equation [16]:

$$Q = CV_b(1 - e^{-t/RC}) \quad . \tag{2.14}$$

If a large enough resistor is used, change in Q is slow and considered negligible at high vibration frequencies, in comparison to the change in C [17]. Therefore, V_g can be determined by holding Q constant, and calculating the voltage difference between peak locations. Using equations:

$$V = \frac{Q}{C}, \qquad C = \frac{a\varepsilon}{d}, \quad \text{and} \quad V_0 = V_b \quad ,$$

the derivation goes as follows.

$$\begin{aligned} V_1 = \frac{Q}{C_1} &= \frac{Qd_1}{a\varepsilon} \\ V_2 = \frac{Q}{C_2} &= \frac{Qd_2}{a\varepsilon} \\ \Delta V = V_2 - V_1 &= \frac{Qx}{a\varepsilon} \end{aligned}$$

substitution:

$$\Delta V = \frac{Qx}{C_0 d_0} = \frac{V_0 x}{d_0} = \frac{V_b x}{d_0}$$

In order to make β calculations, the peak to peak displacement amplitudes are needed. At the vibrating surface of interest, the free boundary idealization is assumed. When a wave reaches a free boundary, the amplitude becomes twice that of the internal wave [16]. Therefore the correct equation for relating the wave signal amplitudes to sinusoidal voltage amplitudes is

$$V_g = \frac{2V_b A}{d_0} \quad . \tag{2.15}$$

Since C_0 is easier to measure than d_0, we can substitute in Equation 2.12, and solve for amplitude to get

$$A = \frac{V_g a \varepsilon}{2 V_b C_0} \quad . \tag{2.16}$$

2.5 Equivalent Circuit

Although it may not be obvious from Figure 2.1, the sample and ground ring are both at ground, while the detector button electrode is the high side of the capacitive gap after the bias voltage is applied. Since the ground ring is conductive, a sizable capacitance is created between the detector button and the ground ring. Therefore, our idealization of two parallel plates is not accurate. However, the detection system can be modeled as two capacitors in parallel. All undesirable but unavoidable capacitances are termed as stray capacitance (C_s).

A depiction of this equivalent circuit is given in Figure 2.3. What is also necessary for signal detection is a separation box, which includes a resistor and capacitor. By applying the DC bias voltage between the detector and a large capacitor, only the alternating portion of the voltage signal is detected by the oscilloscope. As previously discussed the large resistor is necessary to maintain constant charge Q on the capacitive surfaces.

This circuit is further simplified by replacing it with an equivalent form [3]. By making the separation box capacitance much larger than the detector capacitance, and equating capacitors in series, the larger capacitor becomes negligible [16]. From Figure 2.4, it becomes clear that the stray capacitance can have a definite effect on the measured signal.

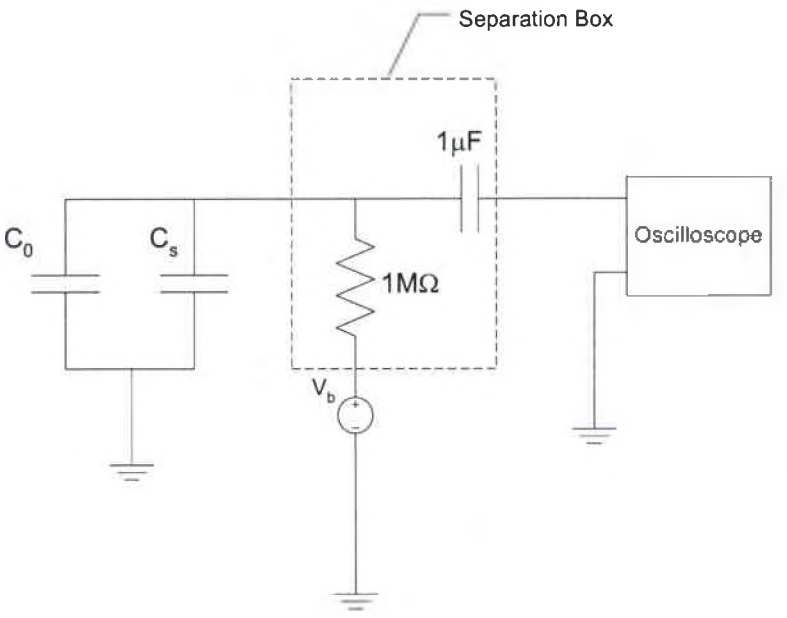

Figure 2.3: Equivalent Circuit For Detector

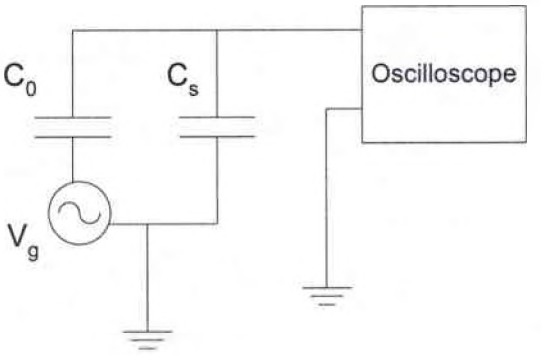

Figure 2.4: Circuit Equivalent for Generated Voltage

The AC generated voltage V_g depicted in Figure 2.4 is the signal of consequence that needs to be determined in order to solve Equation 2.16 for displacement amplitudes. The method chosen for accomplishing this is through a calibration routine using a substitution circuit. The detector is replaced in the circuit by a substitution box containing the components depicted in Figure 2.5. The V_g signal of the circuit equivalent is replaced by an accurate function generator. Through this calibration method, accurate comparisons can be made between the outputs measured and the generated signal that is needed.

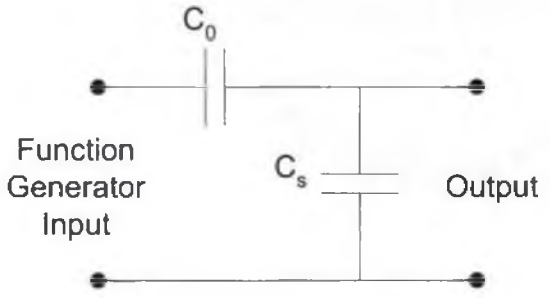

Figure 2.5: Substitution Circuit for V_g Calibration

2.6 Theory Summary

To summarize the theory used for β parameter measurements, it is of use to review all of the measured values used in the necessary equations. The raw β calculated from Equation 2.3 necessitates a value for the sample length l and the wave number k determined from the wave frequency and velocity. The radius r of the piston source, and the attenuation coefficients α_1 and α_2 are additional values needed for the β

correction Equation 2.11. Finally, the capacitive gap permittivity ε, bias voltage V_b, static gap capacitance C_0, and calibrated generated voltage V_g values are also needed for the A_1 and A_2 calculations from Equation 2.16.

CHAPTER 3

METHOD FOR β MEASUREMENT ACQUISITION

In theory, β measurements may sound straight forward and trivial, however, this is not the case since much care in test setup and extensive measurements are needed to assure accuracy. The calculation of β only requires a measurement of A_1, A_2, path length l, and wave number k. Not only are these measurements derived from multiple other measurements, but repetitions are needed for averaging purposes. Along with the tedious nature of these measurements, comes the special attention required for sample preparation, test setup, and wave signal recognition. This chapter seeks to provide an understanding of how one can obtain β readings.

3.1 Sample Preparation

Ideally, advancements will be made in the area of nonlinear acoustics that will allow for non-contact methods for β acquisition. The β parameter would then be more practical for use as a nondestructive evaluation technique. Another goal, in route to practical usefulness, is to be able to identify and characterize the effect of surface features such as geometry, residual stresses, and oxidation. In order to accomplish this, 'real world' surfaces must be compared with 'controlled' surfaces. For the capacitive detection technique, a 'controlled' sample is one with flat, polished, parallel, and stress free surfaces.

3.1.1 Removal of Material

After the sample of interest is machined or otherwise processed into its general shape, the first step of preparation is the removal of the disturbed surface material. If the surfaces have residual stresses as result of being shot peened, electro-discharge machined, or rough machined in some other manner, 200 μm or more of material must be removed. If the opposing surfaces in the direction of signal propagation are not parallel, material also must be removed until parallelism is achieved.

The method of choice used was through grinding on different grits of Silicon Carbide paper on a rotating wheel [3]. This procedure also induces stresses, but through consecutive steps of increasingly finer grit paper, acceptable levels can be achieved. At intervals, the thickness is monitored at multiple locations to check for even, parallel, and appropriate amount of material removal.

3.1.2 Lapping Procedures

At this stage, if deep scratches exist on the surface, polishing with different levels of diamond suspension fluid over TexMet cloth on the rotating polishing wheel may be necessary. Otherwise, it is possible to proceed directly to the final preparation stage of surface lapping. The purpose of this step is to create a smooth surface that is both flat and free of noticeable scratches.

To achieve flatness, successive levels of decreasing sized diamond paste rubbed gently and thinly across a sheet of glass. Common sheets of glass from a hardware store are by nature extremely flat. Therefore, if the sample is lapped on the glass surface in a manner of intimate contact, good flatness is achieved. The glass must be thick enough however, not to deform under applied lapping pressures. Through trial

and error, applying the paste extremely thin and well dispersed across a dry surface has been found to allow for the most intimate surface contact and, respectively, the best flatness. Cleaning the glass thoroughly between different grits of diamond paste is also important to properly avoid scratches. The final step is to move the sample by hand across a TexMet pad on glass with one micron or finer diamond paste. This provides for a smooth reflective surface.

3.1.3 Flat and Parallel Surfaces

The reason for both flat and parallel surfaces is to achieve as best as possible the assumptions made in Chapter 2. The plane of ultrasonic wave initiation is assumed to be detected on the same orientation. Measurements such as attenuation and wave velocity depend on multiple reflections and are therefore affected by non-parallel surfaces [18]. Equation 2.12 for the capacitance of the detector is based on the assumption that two flat parallel plates exist. Therefore deviations could be cause for inaccurate amplitude calculations as well. Typically deviations less than half a degree were possible.

Parallelism is measured simply with an accurate dimensioning tool such as a micrometer, but flatness must be checked through the use of an optical flat. By placing an optical flat on a reflective surface, the flatness can be observed by shinning monochromatic light on to it and inspecting the interference pattern. The distance between interference bands represents a deviation of half the wavelength of the light in distance from flatness [16]. These bands act as a topographical map of the surface, and the further apart the bands, the more acceptable the flatness is. For cylindrical shaped samples, a center ring of one inch in diameter was shown possible. Of note:

it is important to check the flatness of the glass used for lapping first, since this is the limiting factor for polishing.

3.2 Equipment and Test Setup

3.2.1 The Capacitive Detector

The capacitive detector (Figure 2.1) can be divided into three subassemblies: The base, sample platform, and the top drive assemblies.

The base both supports and aligns the other two subassemblies. The BNC connection on the bottom left side of Figure 2.1 is the output connection for both capacitance and signal measurements. The resistor and BNC connection on the opposite side of the base were necessary for a previous calibration technique and are no longer used. Three threaded rods are embedded around the outside of the base for stabilization and alignment of the drive assembly. The banana jack receives the button connection from the sample platform and provides the high side of the circuit for the bias voltage. The rest of the base must be properly grounded.

The sample platform assembly includes the detector electrode button, a ground ring, and a conducting path to the banana jack. This subassembly is removable from the base, allowing for interchangeable platforms of different button diameters. The inner conducting path is well insulated from the outer grounded material. The surfaces of the ground ring and the button must be polished flat simultaneously. By subsequently inserting a thin foil ring between the optical flat and its seat in the ground ring, the button is recessed a depth equal to the thickness of the foil. Recessed depths of 5 μm and smaller are possible. An optical flat can be used again at this point to check for both flat and parallel surfaces.

To apply an input signal across the piezoelectric crystal, the drive assembly must make ground contact with the sample, and high contact with the top of the crystal. This is accomplished by using a spring loaded contact with the crystal transducer. The outer ground material rests on the sample and is insulated from the signal transmit path. The entire drive assembly is tightened down by nuts and springs on each of the three threaded rods. The BNC connection on top is simply connected to the input electronics for ultrasonic wave creation.

3.2.2 Support Equipment and Schematic for Capacitive Detection

Although the detector is the main special purpose piece of equipment for β measurements, many other electronic items are needed. First, equipment is needed for creating an electric signal of the desired pure frequency to be propagated through the material. Then, equipment is needed to separate the fundamental and second harmonic frequencies, and measure amplitudes. Lastly, more electronics are required for calibration of the detected signals.

As can be seen from Figure 3.1 and Table 3.1, the function generator drives the input of the ultrasonic wave. After the electronic signal is amplified and frequency filtered, it is applied across a piezoelectric crystal. Since the initial signal is generated as a sinusoidal N-cycle burst wave, the longitudinal displacement wave created by the crystal is the same.

The output signal includes both the fundamental and other higher order harmonic frequencies. The fundamental signal amplitude is measured directly by the oscilloscope since the second harmonic is much smaller and can be neglected. To measure

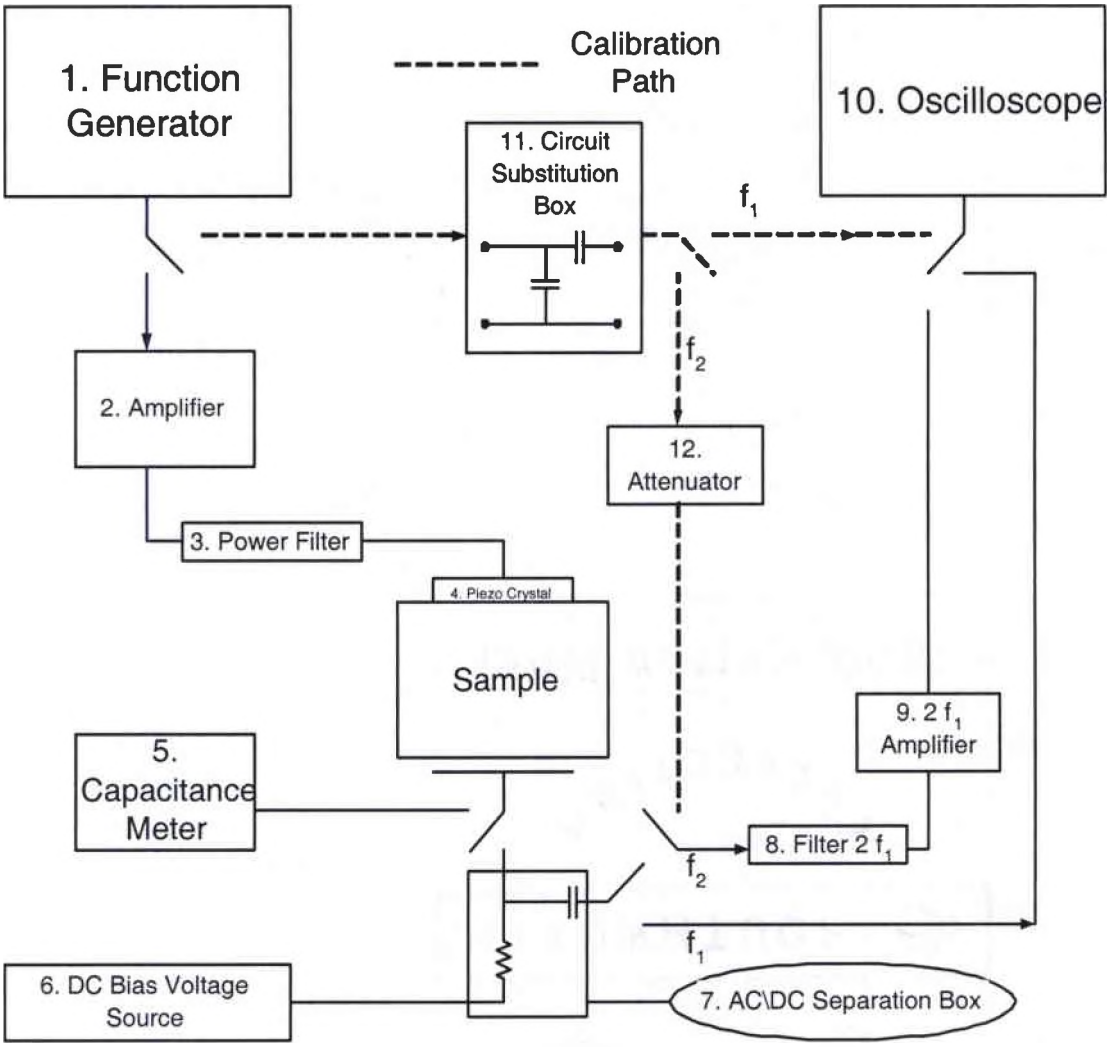

Figure 3.1: Flow Chart of Equipment for β Measurements

the second harmonic however, the signal must be extracted through a band pass filter and amplified before being sent to the oscilloscope.

Other equipment is needed for either calibration or miscellaneous detector operations. For the calibration, an equivalent circuit component must be substituted in place of the detector. An attenuator is needed to calibrate for the second harmonic, since a normal function generator is unable to reproduce amplitudes as small as the original operation range. A capacitance meter is used for measuring the capacitance of the detector, and a bias voltage source is needed to operate the detector.

3.3 Measurement Procedures

3.3.1 Preliminary Measurements and Setup

A number of preliminary measurements must be taken before the actual ultrasonic tests are conducted. First, length measurements of the sample are necessary to know the path length of ultrasonic signal propagation. We usually used simple calipers

Table 3.1: Equipment Used in Support of the Capacitive Detector

Ref.#	Item	Description
	Ultrasonic Input	
1.	Agilent 33250A	N-Cycle Waveform Generator
2.	Amplifier Research 150A1008	150 W 10 kHz - 100 MHz Broad Band Amplifier
3.	FSY Custom Built	5 or 10 MHz Band Pass Power Filter
4.	$LiNb_3$ Crystal	36° Y-cut Piezoelectric Crystals
	Misc. Input/Output	
5.	HP 4278A	Capacitance Meter
6.	Agilent 6634B	0-100 V DC Power Supply
	Signal Output	
7.	Built in House	AC/DC Separation Box
8.	FSY Custom Built	10 or 20 MHz Low Power Band Pass Filter
9.	Miteq	10 or 20 MHz 80 db Amplifier
10.	LeCroy Wave Runner LT342	Digital Oscilloscope
11.	Built in House	Circuit Substitution Box w/ variable capacitors
12.	Agilent 355D	0-120 dB VHF Attenuator

or a micrometer, but typically for thicker samples an accuracy to half a millimeter is all that is needed due to the inherent scatter of β readings. A number of the tests reported in this thesis were conducted on samples as thin as 2 mm. In such cases, more accuracy is needed, but as will be discussed later, other variables make β measurements on thin samples less accurate. A number of measurements are taken in different locations within the area of interest to check for parallel surfaces as well.

Two other quantities that need to be measured are the stray and total capacitances of the detector. The stray capacitance (C_s) is the capacitance that exists within the detection unit when no sample is present. The evaluation of stray capacitance is accomplished by attaching a capacitance meter (Figure 3.1 and Table 3.1) to the BNC out (bottom left side in Figure 2.1). After the sample is placed on the detector platform and tightened down with the top drive assembly, the capacitance is remeasured and recorded as the total capacitance (C_t). The static gap capacitance (C_0) created between the sample and the detector electrode is the quantity needed for Equation 2.16. Since C_0 is in parallel with C_s (see Figure 2.4), $C_0 = C_t - C_s$.

To properly integrate a sample into the detector setup, the piezoelectric crystal must first be bonded to the top surface. In this research the crystal was coupled with a phenyl salicylate solid bond. The sample is then set onto the detector button ground ring with the crystal coaxially aligned over the detecting electrode. The drive assembly is gently brought into contact with the crystal and top surface of the sample and then tightened down. After the total capacitance is determined, the input and output electronics are connected.

3.3.2 Ultrasonic Measurements

Once the preliminary measurements are completed and the input and output circuitry is attached, the test is ready to run. The function generator is turned on and set to produce a sinusoidal, N-cycle bursting, electronic signal. After amplification, filtering, and application of this signal across the $LiNb_3$ crystal, a pure frequency ultrasonic signal is introduced and propagated through the sample. An example signal detected by the capacitive gap transducer is shown in Figure 3.2.

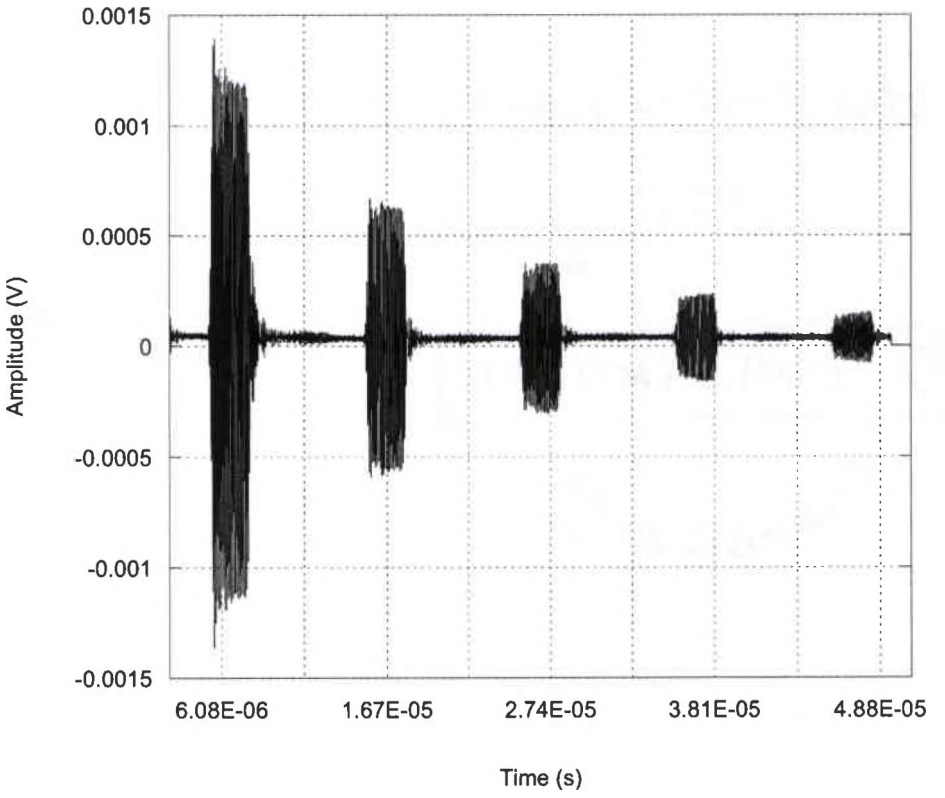

Figure 3.2: Example of a Detected Fundamental Signal

Before measuring the amplitudes, the signal is inspected for correct tuning of the crystal, minimal feedthrough signals, and proper wave pattern. The resonant frequency of a crystal can be measured with a network analyzer, but once bonded the actual tune may be a little different. Further discussion of tuning is given in Chapter 4. In some circumstances, such as incorrect grounding, poor bonding of the crystal, or weak electrical contact to the crystal, feedthrough signals or incorrect wave patterns will exist. In such cases, the test setup must be redone. When the setup is correct, the input frequency matches the tune of the crystal, the cycle count of the burst is low enough that reflected waves do not overlap, and each echo burst fits an exponential decay curve (see Figure 3.2).

The desired readings to obtain from the oscilloscope are the peak to peak voltage amplitudes of the fundamental A_1 and generated 2nd harmonic A_2 signals. As shown in Figure 3.1, a different circuit is required for detecting the two frequency signals. Multiple measurements are read off the first received burst as the input voltage is varied. Normally the tests run in this project were measured manually for seven different input voltages ideally across the widest range possible. At high enough amplitudes the crystal becomes saturated with signal and produces undesirable results. With too little input voltage, the signals become too small to detect.

Along with the signal amplitudes, the velocity of the ultrasonic wave through the material is measured through inspection of the fundamental signal. With multiple reflections of the wave burst, corresponding points on two different bursts are marked, and the time elapse between the points are measured. Knowing that the wave travels two lengths of the sample between each echo, the velocity can be calculated as $v = \frac{2l \cdot n}{t}$,

where n equals number of echoes elapsed, and t equals time. In this report, time measurements where made between the first and third echoes.

3.3.3 Displacement Calibration

In this project, data collection and calculations were performed using an Excel spread sheet. An example[1] is shown in Figure 3.3. While all of the measurements listed previously are recorded into this spreadsheet, the main calculations can only be performed with calibrated values for the voltage output amplitudes.

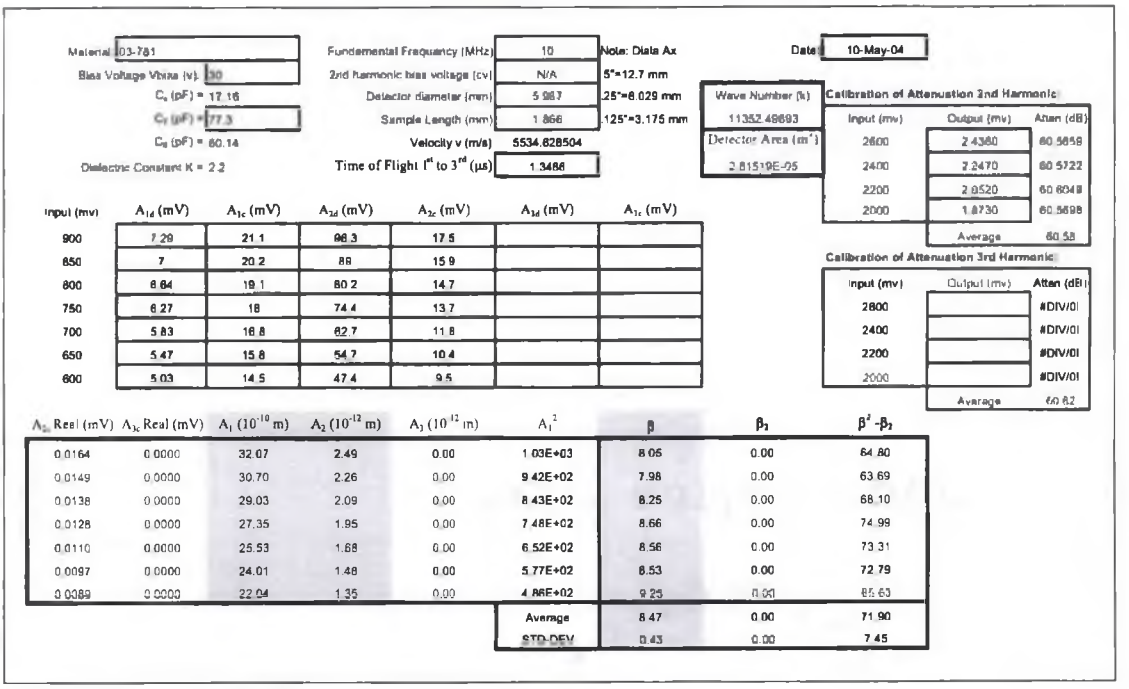

Material	303-781		
Bias Voltage Vbias (v)	30		
C_x (pF) =	17.16		
C_T (pF) =	77.3		
C_s (pF) =	60.14		
Dielectric Constant K =	2.2		
Fundamental Frequency (MHz)	10	Note: Data Ax	
2nd harmonic bias voltage (cv)	N/A	5"=12.7 mm	
Detector diameter (mm)	5.987	.25"=6.029 mm	
Sample Length (mm)	1.866	.125"=3.175 mm	
Velocity v (m/s)	5534.828504		
Time of Flight t^{st} to 3^{rd} (µs)	1.3486		
Date	10-May-04		
Wave Number (k)	11352.49893		
Detector Area (m^2)	2.81519E-05		

Calibration of Attenuation 2nd Harmonic

Input (mv)	Output (mv)	Atten (dB)
2600	2.4380	60.5658
2400	2.2470	60.5722
2200	2.0520	60.6048
2000	1.8730	60.5698
	Average	60.58

Calibration of Attenuation 3rd Harmonic

Input (mv)	Output (mv)	Atten (dB)
2600		#DIV/0!
2400		#DIV/0!
2200		#DIV/0!
2000		#DIV/0!
	Average	60.82

Input (mv)	A_{1d} (mV)	A_{1c} (mV)	A_{2d} (mV)	A_{2c} (mV)	A_{3d} (mV)	A_{3c} (mV)
900	7.29	21.1	98.3	17.5		
850	7	20.2	88	15.9		
800	6.84	19.1	80.2	14.7		
750	6.27	18	74.4	13.7		
700	5.83	16.8	62.7	11.8		
650	5.47	15.8	54.7	10.4		
600	5.03	14.5	47.4	9.5		

A_{1c} Real (mV)	A_{1c} Real (mV)	A_1 (10^{-10} m)	A_2 (10^{-12} m)	A_3 (10^{-12} m)	A_1^2	β	β_3	$\beta^2 - \beta_3$
0.0164	0.0000	32.07	2.49	0.00	1.03E+03	8.05	0.00	64.80
0.0149	0.0000	30.70	2.26	0.00	9.42E+02	7.98	0.00	63.69
0.0138	0.0000	29.03	2.09	0.00	8.43E+02	8.25	0.00	68.10
0.0128	0.0000	27.35	1.95	0.00	7.48E+02	8.66	0.00	74.99
0.0110	0.0000	25.53	1.68	0.00	6.52E+02	8.56	0.00	73.31
0.0097	0.0000	24.01	1.48	0.00	5.77E+02	8.53	0.00	72.79
0.0089	0.0000	22.04	1.35	0.00	4.86E+02	9.25	0.00	85.63
					Average	8.47	0.00	71.90
					STD-DEV	0.43	0.00	7.45

Figure 3.3: Example Spreadsheet for Data Collection and β Calculations

[1]The spread sheet used was initially created by Eric Burke [15].

The cells at the top of the spread sheet contain the preliminary measurements while the center block of cells contains the test results. The voltage amplitudes from the detector, A_{1d} and A_{2d}, are recorded in the first and third columns. To calibrate these values the signal detection path is replaced with the calibration path as shown in Figure 3.1. The amplitude from the function generator is varied until the measured output equals the value of the originally detected amplitudes. The resulting amplitude required from the function generator is the calibrated value, A_{1c} or A_{2c}, and it is recorded in column two or four. The block of cells at the bottom of the spread sheet contains all of the necessary computed results. The columns for displacement amplitudes A_1 and A_2, and for β results are highlighted in Figure 3.3. Some columns shown in this spread sheet were used at one time with third harmonic measurements but were not used for the current research.

To verify that β is independent of input voltage sent to the piezoelectric transducer, A_2 can be plotted versus ${A_1}^2$. If the theoretical β equation is valid, a good linear fit should result. Typically, the seven resulting β values are averaged and reported along with a standard deviation.

CHAPTER 4

β CHARACTERIZATION IN HIGH TEMPERATURE FATIGUED WASPALOY

Previous to the current research, Eric Burke [15] had performed an investigation on the applicability of nonlinear acoustics to detect fatigue damage in nickel-base superalloys. A significant part of the current work was to extend this previous research.

4.1 Summary of Previous Research

To fully review the previous work, please refer to the original reference [15]. Here, only a summary of the research concerning Waspaloy interrupted fatigue tests is important. Dog bone specimens were machined and fatigue tested at 649°C using a servohydraulic test machine. By loading one specimen until failure, a standard cycle count for complete life was established. Other specimens were then loaded and interrupted for β measurements at 0 and 1 cycle, and at 25%, 50%, and 75% of the life of the previously failed specimen. Through tests on six different specimens, four β values were gathered for the condition "as received", three for 1 cycle, and three for 25% of life, while only two values were gathered for 50% of life and one value for 75% of life. Table 4.1 lists the results. Specimen A, the standard mentioned earlier, was loaded until failure to establish a nominal cycle count for 100% life. Specimen B was exposed to temperature alone, for time periods equivalent to the corresponding fatigue cycles, to understand temperature effects on β. At the conclusion of the

research, four specimens, one for each life cycle representation, were passed on to the current work for further evaluation. The results showed a consistent trend of increasing β versus number of fatigue cycles, but one goal of the current research was to gather more data for the upper stages of life.

Table 4.1: β Fatigue Results of Previous Research [15]

Specimen	As recieved	1 Cycle	25%	50%	75%
A (Life Standard)	7.07				
B (Temperature)	8.15	10.67*		10.29*	
C		10.38			
D			11.22		
E	8.22	9.46	10.87	12.72	
F	7.84	10.88	10.33	12.63	14.62
Average	7.82	10.17	10.81	12.68	14.62

* Exposed to temperature for length time corresponding to equivalent cycle time.

The research also reported a β map across the gage length for the 75% life representation specimen (see Figure 4.1). The mapping results were peculiar in that a peak value was demonstrated in the exact middle of the gauge length. Past research has reported similar type peaks for other materials [5, 14], but this peak is particularly sharp and sensitive to position. The other goal of the current research was to validate, and or monitor the development of, this peak behavior.

4.2 Conditions for Waspaloy Dog Bone Fatigue Tests

Figure 4.2 [15] shows a picture of a Waspaloy specimen. The overall length of the specimen is 125 mm. The gage section of 20 mm in length, 10 mm in width, and 2 mm in thickness was electropolished to remove any surface residual stresses and provide a smooth scratch free, but not perfectly flat, surface for β measurements. To

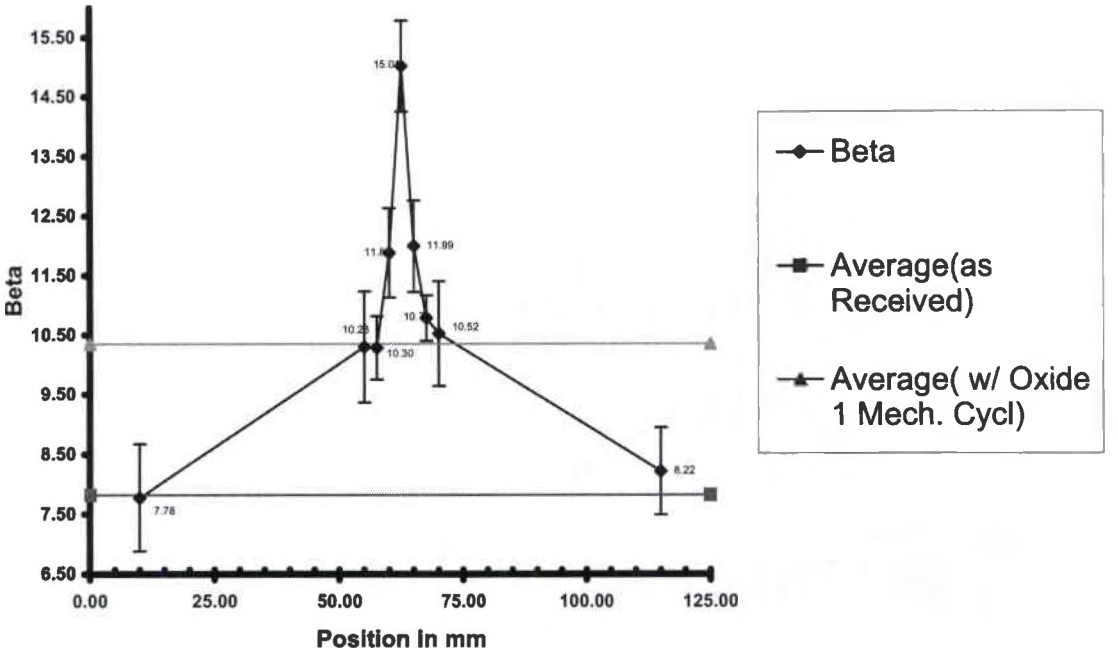

Figure 4.1: β Map of 75% Life Specimen from Previous Research [15]

apply a set of fatigue cycles, the specimens were first heated to a stable 649°C across the gage section. Then, a sinusoidal load pattern of 20 cycles per minute was applied with a maximum stress equal to 1.1 times the yield stress with $R = 0.05$.

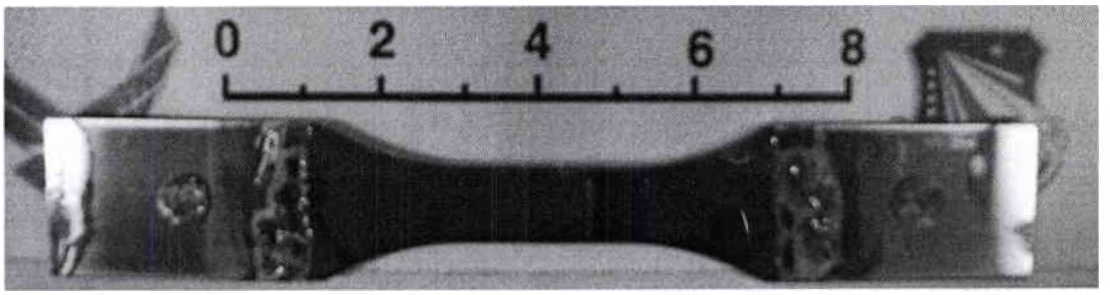

Figure 4.2: Typical Electropolished Waspaloy Dog Bone Specimen

Consistent conditions were maintained when measuring β values for the dog bone specimens. Beta measurements were conducted at a fundamental frequency of 10 MHz. Since the wave propagation distance in the Waspaloy specimens was short, i.e., the specimens were relatively thin, the amplitudes of the harmonic signals were unusually small. To amplify the harmonic signals, air was replaced by Diala Ax oil as the dielectric in the capacitive gap. Diala Ax has a dielectric constant of 2.2 which results in stronger signals. To avoid wave overlap within the 2 mm thick specimens, a wave burst no larger than 4 cycles was necessary. Even though filters gave the input sinusoidal wave burst a rounded envelope (see Figure 4.3), an average of the 4 cycles was attempted in the earlier research for amplitude measurements. For this report, amplitudes were measured from maximum peak values for consistency purposes. Amplitude measurements for thin specimens are discussed further in Section 4.3. A $\frac{1}{4}$ in. diameter 36^o Y-cut $LiNb_3$ crystal was used as the piezoelectric input transducer. Consequently, a $\frac{1}{4}$ in. diameter capacitive receive transducer was also used. The $LiNb_3$ crystals were bonded using phenyl salicylate.

4.3 Complexities in β Measurements

Before the current fatigued Waspaloy tests and results are discussed, a number of β measurement complexities, discovered after the work in reference [15], are noted. First, many issues have arisen regarding our techniques for β measurements. Secondly, locational anomalies have been recognized in the previously reported results of reference [15].

4.3.1 β Measurement Complexities

One of the main discoveries made was that liquid dielectrics are not as well understood as originally thought. The golden standard for capacitive detection of displacement is to use air as the dielectric. While the previous research [15] showed nearly identical β values for the two methods through limited measurements, data since have shown that many discrepancies can exist. When using liquid dielectric material, results can vary whenever differences exist in the capacitive gap conditions between measurements. Dependence of β on capacitance is sometimes evident as discussed in the next section. Changes in the sample surface at the capacitive gap have also shown to affect β. Issues are not fully understood, but vibration damping, mechanical transfer to the liquid and possibly the detecting transducer, and interference

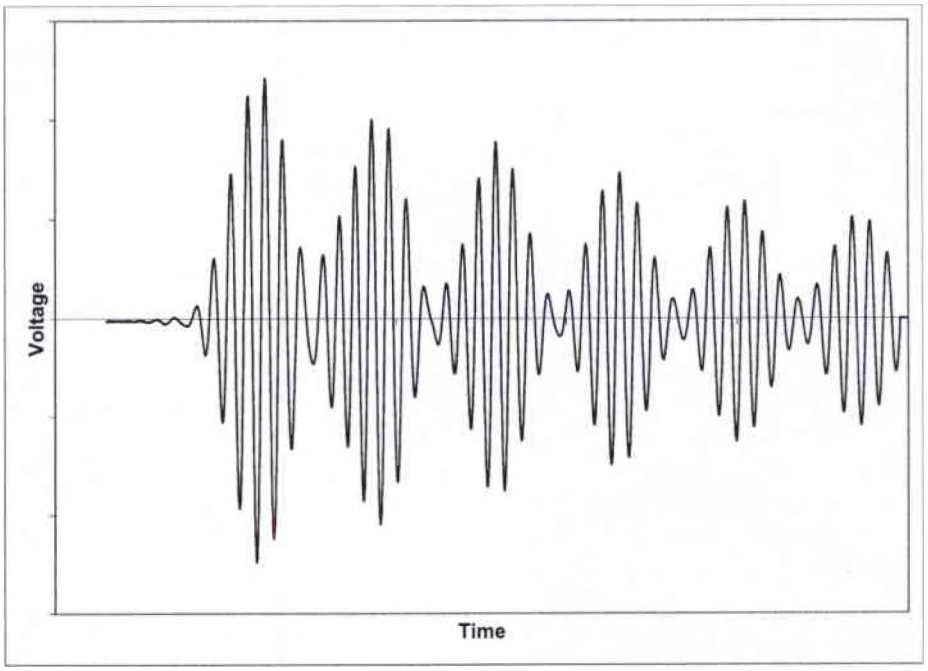

Figure 4.3: Example Wave Pattern for Dog Bone Specimen β Measurements

from the resulting wave reflection in the liquid may all be significant but complex contributions. Since measurements with liquid dielectrics are difficult to understand, comparisons between values can only be made when all the conditions of the capacitive gap, the sample shape and material, and the input signal are kept consistent. These issues are not a problem when using air as the dielectric, where the dielectric constant equals one and very little mechanical transfer exists through a gas.

Tuning issues were discovered to have a significant influence on β. The input piezoelectric crystals have a resonant frequency that is not always identical to the nominal frequency. When setting up the input drive signal for a given β measurement, tuning to the correct frequency was found to be quite difficult since amplitude maximums existed at multiple frequencies. To better understand the tuning process, amplitude measurements and corresponding β values were taken across a sweep of frequencies for a 10 MHz $\frac{1}{4}$ inch crystal. Using a 50 mm thick cylindrical aluminum sample with very little signal attenuation, the resulting measurements were plotted in Figure 4.4.

Partly due to the response of the filters used, two local maximum values were identified for both the fundamental and harmonic signals. When varying the frequency to perform a typical tune, the fundamental signal A_1 is the easiest to monitor, but the harmonic signal A_2 can be monitored as well. Theory predicts that as the fundamental signal varies in amplitude, the second harmonic should vary proportionally to the square of the fundamental amplitude2.3. However, for uncertain reasons, the data in Figure 4.4 show differently. While both the fundamental and second harmonic signals demonstrate corresponding local maximas around 11.2 MHz, the respecitive local maximas do not correspond to each other at a lower frequency around 9.5 MHz.

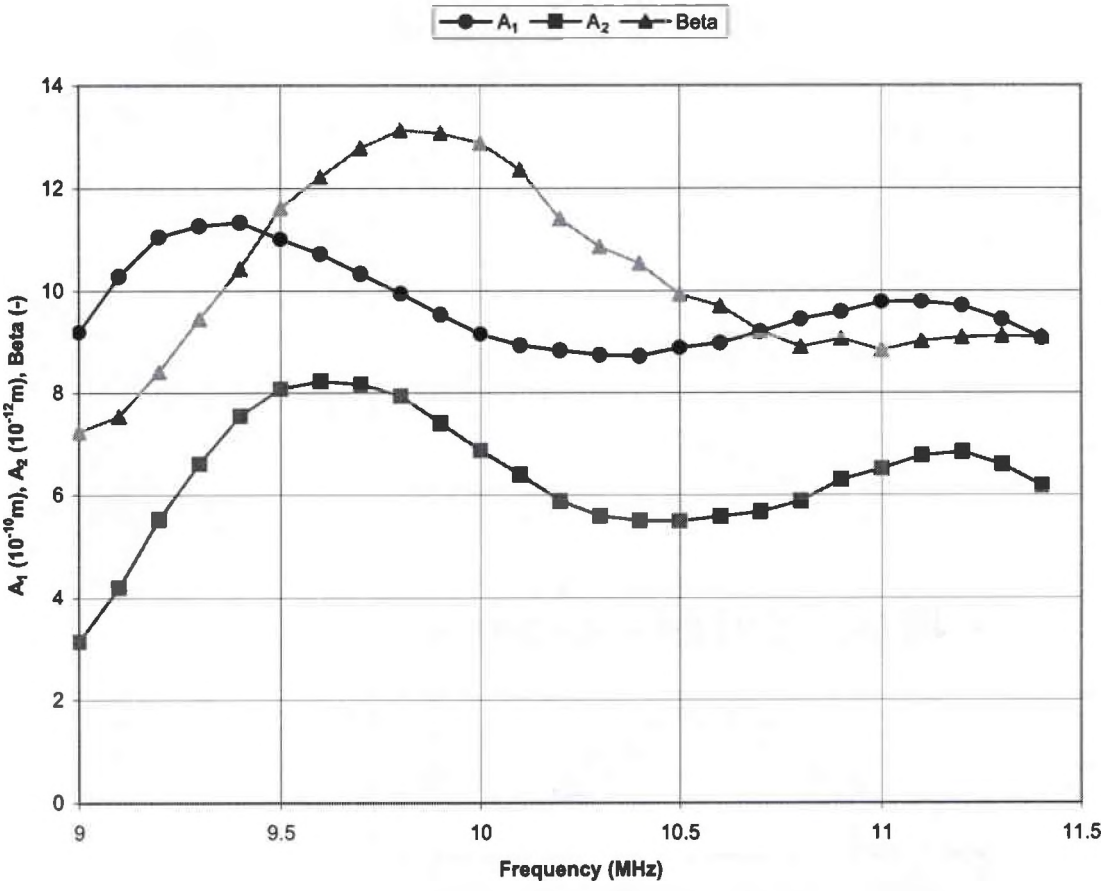

Figure 4.4: Frequency Dependence of β for a 10 MHz 1/4 in. Crystal

Since β is proportional to $\frac{A_2}{A_1^2}$, β becomes highly dependent on frequency near the misalignment of maximas. While avoiding this frequency region altogether is tempting, crystal resonant frequency measurements, taken with a network analyzer, showed energy absorption peaks near the lower frequency maximums. Tuning characteristics can vary with every crystal, bond, and even sample material. Therefore, a tuning procedure was established to first find a frequency that aimed for the peak β value, and then secondly to maintain the same test frequency (and crystal if possible) for all β measurements within a given test matrix.

The other complexity encountered was in trying to apply β measurements to thin samples. While thin sample difficulties had been identified in the previous research [15], a different approach for measurements was taken in the current work. Again, refer to Figure 4.3. For thin specimens, signal reflections can easily overlap and result in wave interference. To avoid overlapping in the 2 mm thick Waspaloy specimens, wave packet burst signals are input at only four cycles per burst. For comparison, 20 or more cycles per burst were often used for thicker specimens. Since amplitude measurements were always taken from the first detected burst in a wave train, a zoomed in version of Figure 3.2 becomes helpful and is shown in Figure 4.5. As shown in the 25 cycle burst, the first four cycles are not a good representation of the entire burst. For this reason, β comparisons between extremely thin samples and thick samples should not be attempted. In the current research, peak amplitude values instead of "averages" were used with four cycle burst measurements for simplicity and consistency between measurements. Of note, the peak to peak measurement method typically results in a 20 percent decrease in β when compared to the previous averaging method.

4.3.2 Complexities with Previous Results

At first glance, the previous β results [15] appear to show promise for characterization of life, but further inspection reveals locational difficulties that make the results less helpful. If for example, such a β peak as shown in Figure 4.1 were common in a Waspaloy disk, it could be very difficult to find. By moving just 2 mm in any direction from the peak, the β value could drastically change. In Table 4.1, the temperature exposed Specimen B, exhibits a jump in β from 8.15 to 10.67 after the equivalent temperature exposure of 1 cycle. 10.67 is the same general value as four out of the six values surrounding the mapped peak β in Figure 4.1. Therefore, the β value for most of the 75% life specimen gauge section has not changed since the beginning of

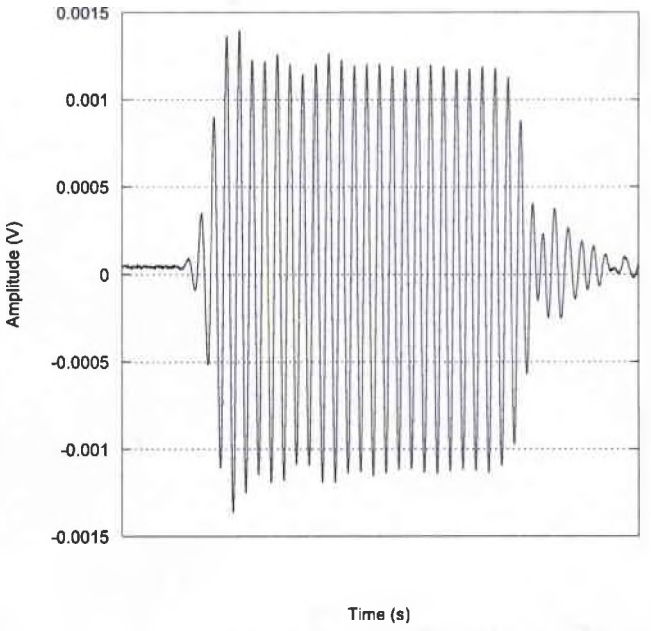

Figure 4.5: First Detected 20 Cycle Burst in a Typical Wave Train

life. The reported increasing trend of β with fatigue cycles would consequently not be true for all portions of the gauge section.

One other significant result to note is that Specimen F, used for the β map, did not ultimately fail in the middle but at the outer edge of the gage section. This indicates that a β peak does not necessarily represent a future failure. Crack initiation and acoustic nonlinearity must often develop by separate mechanisms. Also, specimens C, D, and E all failed well before the standard cycle count for 100% life. Therefore the percent life characterizations reported are somewhat deceptive and not always applicable.

4.4 Fatigue Testing Continued on Dog Bone Specimens

As stated before, the 1 cycle and 25%, 50%, and 75% of nominal life specimens from the previous research were utilized for additional testing. Unfortunately, three of the specimens failed within the next loading series of cycles, and the fourth failed soon after. Also, many of the complexities reported in Section 4.3 were discovered while attempting β measurements on these specimens. For these reasons, little confidence was established in the few β values gathered, and none of the values are reported.

Therefore, another specimen, labeled G, in the "as received" state was found and fatigue loaded. Fatigue tests were interrupted for β readings at 0, 1, 12125, 18556, 29956, and 36000 cycles without reaching specimen failure. β values were measured at multiple locations to monitor the growth of any peaks. The β results are displayed in Table 4.2. Again it is important to note that these values cannot be compared directly to those of the previous research because signal amplitudes were measured differently and capacitive gap conditions may be different.

Results show that not only was there no identifiable peak within the gage section, but little increase of β with fatigue cycles was also demonstrated. While these results differ from those reported in the previous research [15], they are not completely inconsistent. As discussed earlier, little change in β probably occurred in most of the gage section for the previous specimens as well. Theoretically the entire gage section should be under the same stress conditions, and dislocation buildups could be expected relatively homogeneous with respect to the volume measured beneath a 1/4 in transducer. Therefore a β peak would not be expected. If a peak were common, it should be random as to location within the gage section.

At this point in the research, Specimen G had not failed despite reaching the nominal measure for 100% life. However, a possible crack was observed along the edge however. Since the crack was outside of the gage length, a new detector button with a smaller ground ring was created to allow β readings near the electropolished lip present on the dog bone specimens. Figure 4.6 shows the β results along the center and along the specimen edge near the crack. The crack was located at 76 mm, but no significant change in β was detected. Of note, even though a different detector button

Table 4.2: β Results for Specimen G

Location (mm)	As recieved	1 cycle	12,125 cycles	18,556 cycles	29,956 cycles	36,000 cycles
50.0						8.30
54.0		6.96	6.42		7.79	7.65
57.5	6.16	6.78	7.30	7.09	8.26	8.06
60.0						8.36
62.5	5.80	6.82	8.68	7.41	8.35	7.87
65.0						7.75
67.5	6.52	8.37	7.65	7.93	7.15	7.41
71.0		6.74	7.10		6.81	7.85
76.0						7.06
Average	6.16	7.13	7.43	7.48	7.67	7.81

was used to measure β along the edge and at the outermost centerline locations, the capacitive gap conditions were probably similar to have allowed for comparable results with the larger original button.

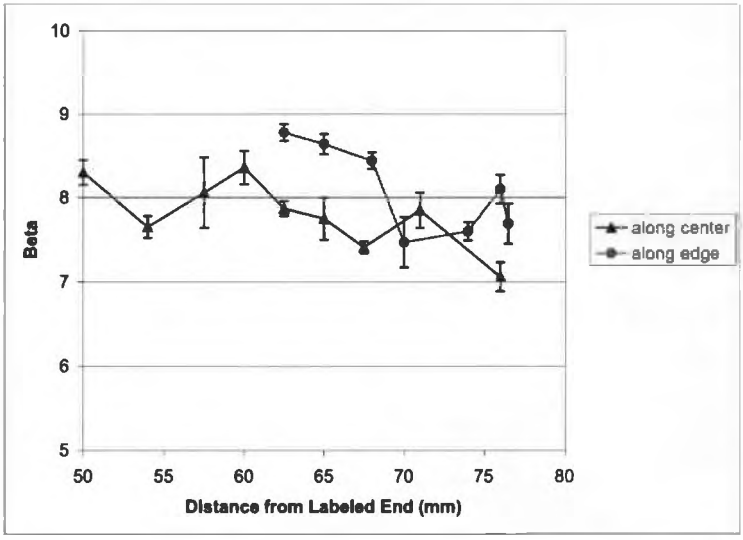

Figure 4.6: Map of Beta across Specimen G at 100% life

Further fatigue loading and β measurements were performed, but unfortunately the tests were not continued until after the disk samples of Chapter 5 were evaluated. In the process of making β measurements on the disk samples, the larger ground ring capacitive detector button was changed. Accordingly, subsequent liquid dielectric β measurements can not be directly compared to the previous values. Fortunately though the smaller ground ring detector button was still in its original condition. Therefore, β measurements were acquired with both buttons for comparison purposes and are reported in Table 4.3. All the β values were read in the very center of Specimen G.

The results shown in Table 4.3 demonstrate two things. First, the β values still do not appear to be changing significantly with fatigue life in the middle of Specimen G. Secondly, the results provide a good example of how complicated liquid dielectric measurements can be. Upon further investigation, the discrepancies in β readings between these two detector buttons may be largely due to differences in the resulting capacitances. Figure 4.7 shows a plot of β versus the capacitance measured for each measurement. Because of the other complexities of liquid dielectric measurements, an obvious dependence on capacitance, such as with this example, is not always observed.

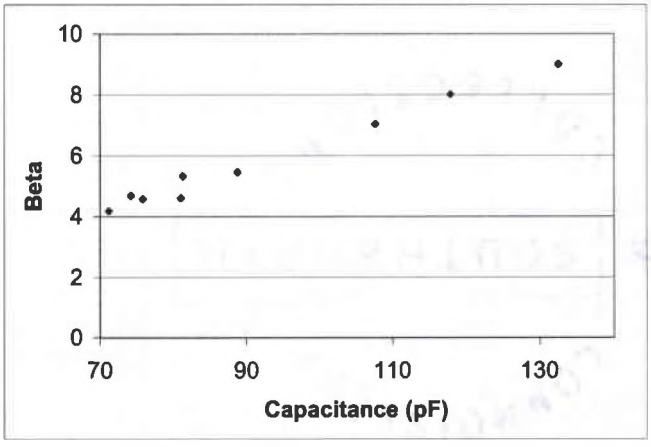

Figure 4.7: Example of β Dependence on Liquid Dielectric Gap Capacitance

Table 4.3: Additional β Values for Specimen G Past 100% Life

Cycle Count	38,000	40,000	42,000	44,000
Large Ground Ring Button	4.61	4.69	5.33	4.18 , 5.46
Small Ground Ring Button	9.00	8.01	7.04	

CHAPTER 5

APPLYING β MEASUREMENTS TO ENGINE COMPONENTS

One of the main goals for this research is to determine the feasibility of applying β measurements toward the life prediction of aircraft engine components. That is, can β be used to assess the fatigue damage state of a component and provide a spatial correlation with damage in different locations. Actual components present geometric obstacles such as non-parallel surfaces, variable thicknesses, and complicated profiles which must be overcome. A good understanding of surface feature effects such as oxidation, surface roughness, and residual stresses are also necessary for practical application.

5.1 First Stage Turbine Engine Disk Samples

To better understand the usefulness of β in evaluating engine component life, a first stage turbine engine disk made of IN-100 was chosen for investigation (see Figure 5.1). Multiple samples were cut, for capacitive detection of β, from two available disks having different cycles when removed from service. Samples from three forgings of the same material, considered as a virgin baseline, were also available. The purpose behind evaluating samples from different sources is to get a representation from three different stages of life.

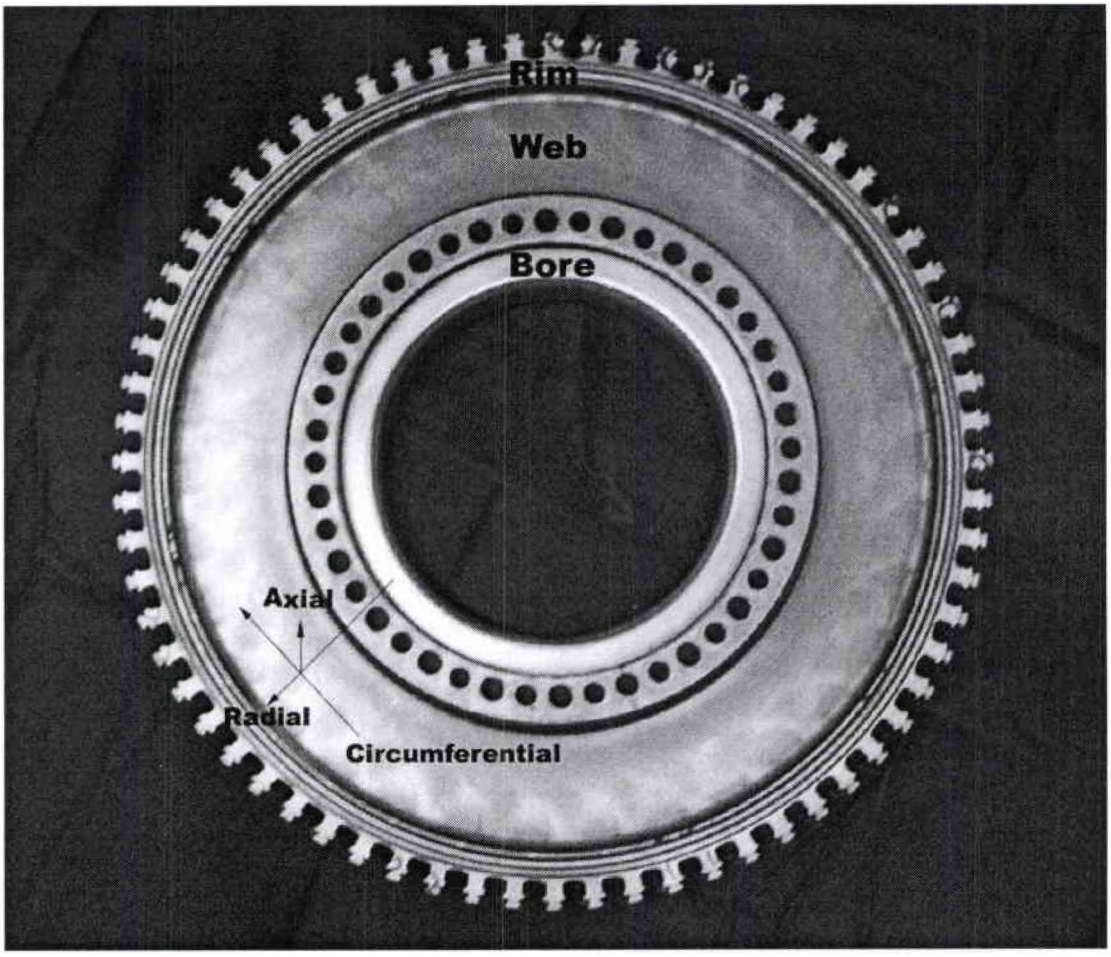

Figure 5.1: First Stage Engine Disk

A test matrix was established and the corresponding β readings were taken (see Table 5.1). All samples were categorized into three general regions: bore, web, and rim. Each sample was then mapped for its axial, circumferential, and radial directions. The "Test" column of Table 5.1 lists all the β values to be measured where B, W, and R (bore, web, and rim) stand for the region; A, C, and R (axial, circumferential, and radial) stand for the direction; and subscripted numbers represent different locations. When possible, original surfaces in the axial direction were preserved, as noted in the table, to represent potential field measurement conditions. All other surfaces where polished, as described in Chapter 3, before β readings were taken. The conditions for β measurements were the same as those listed in Chapter 4 for the Waspaloy dog bone tests with one major exception: air was again used as the capacitive gap dielectric instead of Diala AX, providing for reliable data comparisons.

In theory, the forgings represent a "virgin" state of the IN-100 disks, but none of the three forgings were the right size to form a first stage disk. Forgings II and III were identical in shape to each other, but both presented some difficulties. The only sample from Forging II was a very thin slice providing for small amplitude harmonic signals and complex measurements as described in Chapter 4. As determined from previous research, Forging III did not meet the specified tensile yield strength for the material. Why Forging III is lacking the correct yield strength is not fully understood, but in the case that incorrect processing was used, β values could also be effected. Samples from Forging I were nice sized providing for multiple and reliable readings in varying directions. Forging I was yet another disk shape, but the material meets specifications.

Table 5.1: Test Matrix and Sample Descriptions

Sample	Description	Test
	Forging I	
A	Rim cut	R_C, R_R, R_A
B	Rim cut	R_C, R_R, R_A
	Forging II	
C	5mm thick cross section slice	B_C, W_C, R_C
	Forging III	
D	Radial strip cut from the middle containing bore, web, and rim regions	B_C, W_C, R_C
E	Bore cut	B_C, B_R, B_A
	Disk I	
F	12.7mm thick cross section slice	B_C, W_{C1}, W_{C2}, R_C
	Disk II	
G	Bore piece (original axial surfaces)	$B_{C1}, B_{C2}, B_{C3}, B_{R1}, B_{R2}, B_{R3}, B_A$
G_1	Sample G with $\sim$ 4mm of one original axial surface removed and polished	B_A
G_2	Sample G with both original axial surfaces removed and polished	B_C, B_A
G_3	The top cap piece removed from G (one original axial surface)	B_A
H	Bore piece (original axial surfaces)	$B_{C1}, B_{C2}, B_{C3}, B_{R1}, B_{R2}, B_{R3}, B_A$
H_1	Sample H with one original axial surface removed and polished	B_A
H_2	Sample H with both original axial surfaces removed and polished	B_A
H_3	The top cap piece removed from H (one original axial surface)	B_A
H_4	Axially one third section of H_2	B_A
H_5	Remaining two thirds section of H_2	B_A
I	Web cut (original axial surfaces)	W_A
J	Rim cut	R_A
K	Rim cut	R_A

Both engine disks evaluated were taken out of service. From the usage history of the engines, a general knowledge of each disk's respective fatigue life consumption is available. While all disks are taken out of service well before expected failures, Disk I is considered to have experienced 58 % of expected design usage, while Disk II has endured 93 % of design usage. Therefore, the three stages of life represented are virgin (Forgings I, II, and III), low partial service life (Disk I), and high partial service life (Disk II).

5.1.1 Bore Samples

The purpose of the thick bore region in a disk is to bear the majority of the stresses. Therefore, extensive β measurements were taken in the bore region. However, the full importance of correcting β for attenuation and diffraction was not realized until these bore samples were evaluated. Since the samples represented many different path lengths for ultrasonic measurements, raw β values were not meaningful. Although β corrections were not initially performed, the graph in Figure 5.2 obviously showed a dependence of the raw data on path length. Because of the large scatter of values for the shortest path lengths, the β dependence initially was unclear in regards to being linear or otherwise.

To determine the respective effect of diffraction and attenuation, the bore β values were first corrected for each independently, as shown in Figure 5.3. From the graph, both attenuation and diffraction are shown to be important effects and have opposite trends. For this material, attenuation causes the raw values to be low, while diffraction causes the values to be high. The shorter the path length, the less the effects. One

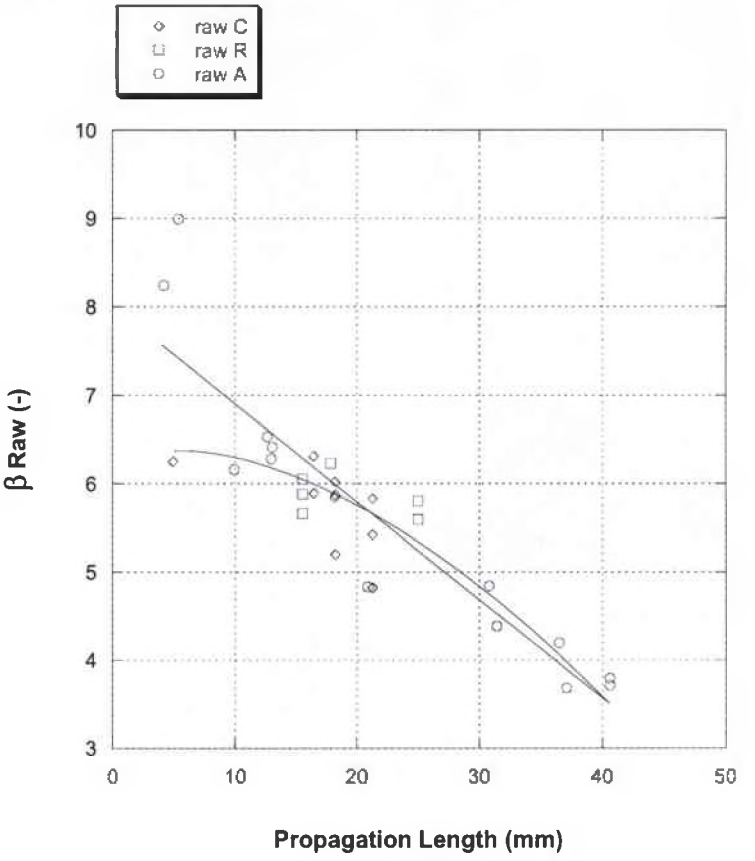

Figure 5.2: Raw β Values for all Bore Samples

other observation is that two values deviate from the general curved trend of path length dependence. The circled values in Figure 5.3 will be discussed later.

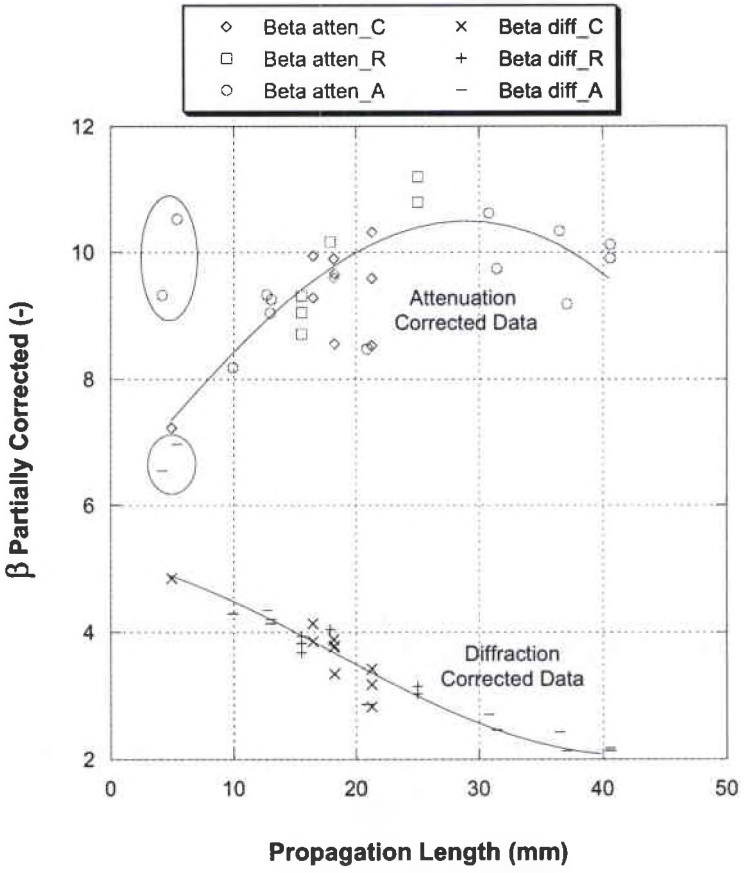

Figure 5.3: Partially Corrected β Values for Bore Samples

Finally, Figure 5.4 shows the fully corrected β values for all the bore measurements. No longer is any path length dependence noticeable. Some variations in values still exist, and the goal now is to determine the sources for these variations. Again, the two obviously different values are circled in Figure 5.4 and will be discussed.

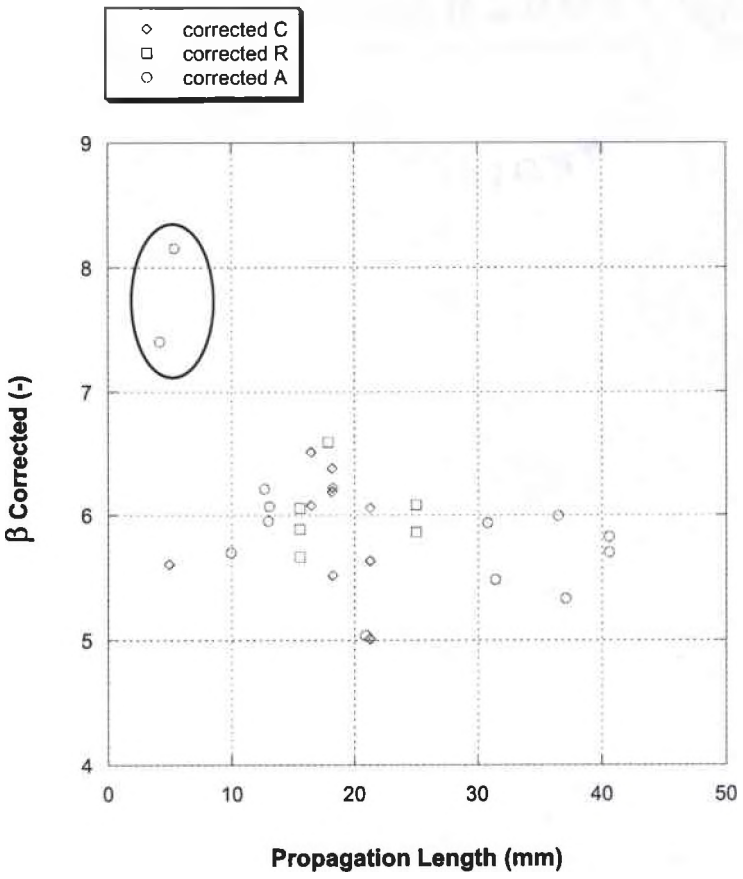

Figure 5.4: All Bore β Values Corrected for Diffraction and Attenuation

5.1.2 Data Analysis

With the corrected β data, a proper analysis can now be performed. Table 5.2 shows all of the corrected β measurements. No consistent pattern was identified for β dependence on direction (as suggested in Figure 5.4, where different symbols represent the circumferential, radial, and axial directions) or on location changes within a given region. Therefore, all the data for Disk II in the bore region (excluding the two uncharacteristic values highlighted in Table 5.2) provide an experimental representation of test variability. Averaged values provide for less scatter, but from one test to another, β is shown to vary by ± 13 % .

Again excluding the two highlighted values, averages are calculated and displayed in Table 5.2. The averages were then used to create the three dimensional plot of Figure 5.5. A few important findings demonstrated in the plot. One, is that a noticeable difference in β exists between Forgings I and II, and Forging III where material property specifications were not satisfied. A possible method for forging quality assurance is therefore present in β values. By throwing out the Forging III data, a β difference is also present between the "virgin" forging material and the service cycled disk material. β values may therefore represent "usage", but as discussed earlier, the tested forgings may not accurately represent a virgin first stage disk. A third interesting finding is that the web values are less than the rim and bore values for every source material, including the forgings. The processing procedures therefore, must be contributing to the higher β in the bore and rim. Lastly of note, the variation of β between the two engine disks, is too small for assigning remaining "life" characteristics. This result is some what to be expected since both disks should be far from life ending failure.

Table 5.2: Data From IN-100 Disk Samples

Source	Sample	Bore	Web	Rim
Forging I	A			4.41
				5.01
				4.68
	B			4.01
				4.64
				3.67
Average				4.40
Forging II	C	5.61	3.90	4.37
Average		5.61	3.90	4.37
Forging III	D	6.08	5.52	6.12
		6.07		
	E	6.51		
		6.59		
		5.95		
Average		6.24		
Disk I	F	6.21	5.43	5.36
			4.91	
Average		6.21	5.17	
Disk II	G	6.38		
		5.51		
		6.22		
		6.08		
		5.86		
		6.08		
		5.82		
	G_1	5.99		
	G_2	6.19		
		5.94		
	G_3			
	H	5.01		
		6.06		
		5.63		
		5.89		
		6.06		
		5.67		
		5.70		
	H_1	5.33		
	H_2	5.48		
	H_3			
	H_4	5.70		
	H_5	5.04		
	I		5.52	
	J			5.82
	K			5.86
Average		5.79	5.52	5.84

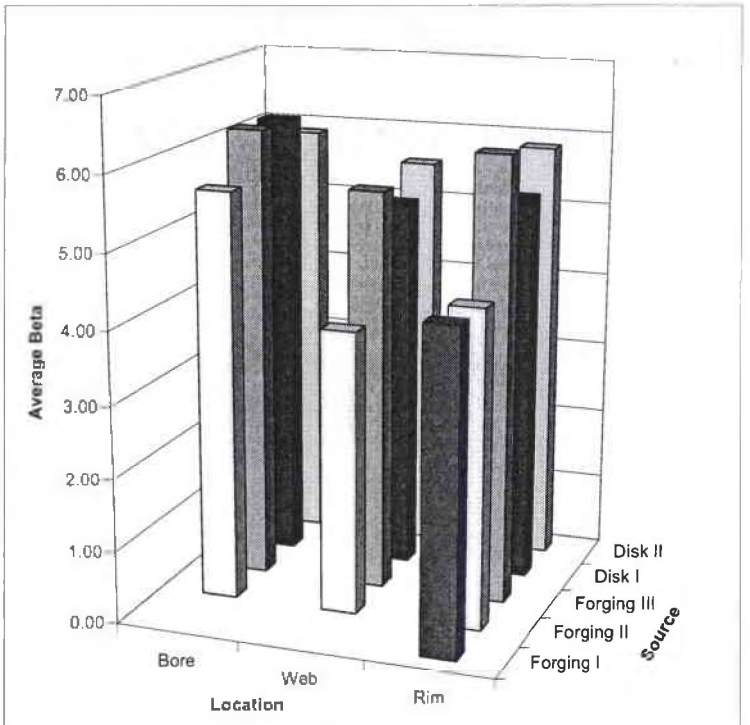

	Bore	Web	Rim
■ Forging I			4.40
□ Forging II	5.61	3.90	4.37
▣ Forging III	6.24	5.52	6.12
■ Disk I	6.21	5.17	5.36
□ Disk II	5.87	5.52	5.84

Figure 5.5: Comparison of Average β Values From all Sources

The most significant test result here may lie in the two uncharacteristic values from samples G_3, and H_3 (the values circled in Figures 5.3 and 5.4, and highlighted in Table 5.2). These two samples were thin, approximately 5 mm thick samples cut from the surface material of the bore samples. If the surface features of oxides, roughness, or state of surface stresses caused the increase in β, one can postulate that some sort of β sum by rule of mixtures is valid. With a rule of mixtures β calculation, longer path lengths would be less effected by the surface material. Since all other disk samples containing original surfaces were 10 mm thick or greater, the fact, that no increase in β was observed, becomes reasonable.

5.2 Shot Peening Specimens and Temperature Exposure

To emphasize again, an oxidized shot peened surface appears to have an increasing effect on the nonlinear β parameter, and all original surfaces measured on the disks were oxidized and shot peened. Since β measurements are considered to be an average value of all the material within the ultrasonic propagation path, the surface effect is minimized for longer path lengths. Questions that need to be answered include: "How thick is the surface layer of consequence?", "What characteristics of a shot peened surface effect β?", and "How does the surface change with exposure to oxidizing high temperature environments?".

A new series of tests were conducted to help answer these surface effect questions. Two small test specimens 4 mm thick were cut from the web region of Disk II. The surfaces were shot peened and β measurements were taken. Since the specimens were thin, Diala Ax oil, exhibiting a dielectric constant of 2.2, was used in place of air in the capacitive gap of the detector in order to increase signal amplitude. In addition to β

values, internal stresses through a surface depth of around 10 microns were measured via X-ray diffraction.

The specimens were then exposed to 649°C in vacuum for 10 hours. Again, β and stress values were measured. As shown in Table 5.3, Specimen I was subsequently exposed to temperature for another 90 hours. The exposure vacuum for Specimen I was not ideal, and a small oxide layer did form on the surface. For comparison, measurements were made with the oxide surfaces and with one surface slightly polished. The word "slightly" is used because only one micron of material removal was needed in order to remove the oxide and the surface roughness.

The results are shown in Table 5.3. Also shown in the table are values for IN-100 2 mm thick dog bone specimens. No fatigue loading or exposure tests were conducted on these specimens, but surface comparisons can be made since one was shot peened and the other was low stress ground. β values were normalized in Table 5.3 to the lowest value in each specimen subset. Normalization was executed in order to allow comparisons between the oil dielectric obtained values with the previous air dielectric values.

The X-ray diffraction stress measurements were performed in five locations on the top and bottom surfaces of the specimens. X-ray diffraction readings were taken before and after performing β measurements. A minimal effect of the β measurement procedure on the residual stresses resulted due to the small amount of heating required to bond a piezoelectric crystal . Since differences were small, all stress readings for the top and bottom surfaces before and after the nonlinear measurements were averaged. Averaging many values was also helpful since a test-to-test scatter band was on the order of 30 ksi.

5.2.1 Relaxation of Internal Stresses

The expected result was that some direct proportionality relationship would exist between internal residual stresses and β. However, the results of shot peened Specimens I and II shown in Table 5.3 appear to indicate that an inverse relationship exists. As the residual stresses relaxed due to exposure to temperature, the β values increased. The two specimens did indicate that a surface effect exists for a shot peened specimen. As the specimens were exposed to temperature, β increased. Then, when one surface was polished, the resulting β was again lower. Since only one micron of material was removed, these results suggest that the surface roughness, especially on the side of transducer bond, may be the major contributor to surface caused β variations.

Since Specimen I was not exposed in an ideal vacuum, a slight oxide layer did develop on the surface. However, the vacuum was improved and no visible oxide was present on Specimen II, yet the same trend in β verses temperature exposure

Table 5.3: Shot Peened Specimen Data

Specimen Condition	β Normalized	Surface Stresses (ksi)
Shot Peened Specimen 1		
As Received	1.00	−143
10hr Exposure	1.13	−12
100hr Exposure	1.19	−5
100hr Exposure (One Side Polished*)	1.01	−30(polished), −5(unpolished)
Shot Peened Specimen 2		
As Received	1.11	−128
10hr Exposure	1.23	−74
IN-100 Dog Bone Specimens		
Low Stress Ground	1.00	−92
Shot Peened	1.51	−108

* Only 1 μm removed

was demonstrated. In the previous work [15], it was proposed that an oxide layer contributed to an increase in β. This research suggests that those results may actually have been caused by a change in surface roughness resulting from the oxide.

5.2.2 Shot Peened vs. Low Stress Ground

The two dog bone specimens with differently prepared surfaces were compared to evaluate surface effects without temperature exposure. At only 2 mm thick, the dog bone specimens should be even more sensitive to surface effects than the 4 mm thick shot peened specimens. While Table 5.3 reports similar stress measurements for the two different surfaces, the shot peened surface stresses are known to exist to a much deeper depth (around 200 microns) than the residual stresses left from a low stress grind. Unfortunately, the X-ray diffraction measurements only penetrated a shallow depth of around 10 microns. Also of note, the shot peened surface appears to be a rougher surface than the visually smooth low stress ground surface.

The measured β value was much higher for the shot peened dog bone as compared to the low stress ground dog bone. Unlike the previous shot peened specimens, the higher β value is matched with the higher (or deeper) residual stresses. However, the higher β value also corresponds with the rougher surface, which is consistent with the previous shot peened surfaces. As a result, the surface roughness appears to be the effect of greater influence. The most probable explanation for this roughness effect must relate to the bond of a flat input crystal to a non-uniform plane surface.

5.3 Potential Use of β for Engine Prognosis

The most important information determined here is that β measurements can be performed with consistency on actual engine disk components approximately 10

mm or more thick. On thin samples, more research should be conducted to fully understand the surface effects, but some general trends have been demonstrated in the present research.

While nonlinear measurements show some potential for quality control in forgings and possibly for detecting deviations from virgin conditions, the sensitivity to engine disk usage doesn't appear great enough for practical engine prognosis. However, nonlinear studies may serve a purpose in helping to quantify a shot peened surface. Much research is being conducted to better understand the benefit that shot peening provides for crack initiation and propagation resistance. While β values may have some dependence on surface roughness, shot peened surface variations due to elevated temperature exposure also appear detectable through β measurements.

CHAPTER 6

CONCLUSIONS

At this point, a discussion of the "absolute" nature of β is beneficial. The literature pertaining to nonlinear acoustics often describes the β parameter in terms of its absoluteness. For a given material in a given condition, only one β value exists. While in theory, this is true, practical applications through measurements are not always as simple. Of most importance to this research, the choice of dielectric material in the capacitive gap proved to have a drastic effect on β. Even when the standard gap of air is used, different frequencies, burst cycle counts, and methods for diffraction correction can lead to differences in β measurements. While comparisons between values can be made when measurement procedures and conditions are consistent, referring to the β values as "absolute" is deceiving.

While many of the measurement difficulties were misunderstood at the start of the current work, consistencies were established, and reliable conclusions have resulted from both the Waspaloy fatigue specimen tests and from the IN-100 engine disk sample measurements.

Waspaloy

Notably, the Waspaloy fatigue tests did not demonstrate much β sensitivity to fatigue life, spacial location, or even to cracks in the current research. While Burke's results did show a β sensitivity to fatigue in one location, the other portions of

the gage length compare similarly to the current results with nonsensitive β values. Even though Burke reports a detected β peak in the material, the specimen failed at a distinctly different location. The main conclusion therefore, is that dislocations and other β-affecting properties often develop by different mechanisms than those influencing crack initiation and ultimate failure in Waspaloy.

IN-100 Engine Disks

The obvious initial conclusion taken from the disk sample results is that β measurements are possible for shot peened oxidized surfaces such as would exist for nondestructive evaluation. Thick samples were unaffected by surface conditions, and consistent comparisons were established independent of sample thickness.

While β sensitivity to life was not proved for IN-100, similar to Waspaloy results, evidence was found for β sensitivity to material processing. Different regions within the disks and forgings resulted in different β values. Also, the "good" and the "bad" forgings provided different β values. Nonlinear acoustic theory does predict lattice effects on β, and future work could be directed toward relating processing, lattice models, and β. Promise therefore exists for β to be used as a measure for quality control of processing.

The final conclusion taken is that surface features have a definite influence on β measurements for very thin samples. Oxidation, shot peened stresses, and temperature exposure may all have effects on β, but surface roughness appears to be the dominant effect. The question arises if even Burke's peak β measurement on Waspaloy might have been caused from a location of surface roughness. Further research needs to be done, but β measurements could be useful in surface analysis of materials.

Future Research

Much has been learned in regards to the nonlinear acoustic parameter β and its applications, but wide fields for future research still exist. To continue with nickel-based superalloy research, an in depth study to compare β values with processing differences would be beneficial. Further research potential exists in the area of characterizing temperature exposed, shot peened, rough surfaces. Surface effect research could also be enhanced by improved β measurement procedures to allow for more consistent thin specimen values.

Two other key areas of research are recommended here. First, the field of nonlinear acoustics could benefit greatly from experimental application to a variety of other solid materials. How β behaves in all materials is not yet thoroughly understood. Lastly, new improved techniques for amplitude detection need to be discovered and developed. Non-contact methods of detection would greatly benefit field inspections. Finer amplitude sensitivity methods would allow detection of higher order harmonics and further acoustic understanding.

BIBLIOGRAPHY

[1] K. Moore, *Encyclopedia of Science and Technology*, vol. 12. McGraw-Hill, 2002.

[2] M. A. Breazeale and J. Philip, "Determination of third-order elastic constants from ultrasonic harmonic generation measurements," *Physical Acoustics*, vol. 17, pp. 1–60, 1984.

[3] W. T. Yost and J. H. Cantrell, "Harmonic generation measurements in nonlinear acoustics." Lecture Notes: Course on Nonlinear Acoustics, at the 2001 IEEE Symposium on Ultrasonics, Atlanta, GA.

[4] J. K. Na, *Ultrasonic Measurement of the Linear and the Nonlinear Elastic Properties of PZT Ceramics.* PhD thesis, University of Tennessee, 1991.

[5] J. Frouin, *Monitoring Linear and Nonlinear Acoustic Behavior of Titanium Alloys During Cyclic Loading.* PhD thesis, University of Dayton, Dayton, OH, June 2001.

[6] D. C. Hurley, W. T. Yost, E. S. Boltz, and C. M. Fortunko, "A comparison of three techniques to determine the nonlinear ultrasonic parameter β," *Review of Progress in Quantitative Nondestructive Evaluation*, vol. 16, pp. 1383–1390, 1997.

[7] B. D. Blackburn and M. A. Breazeale, "Nonlinear distortion of ultrasonic waves in small crystalline samples," *J. Acoust. Soc. Am.*, vol. 76, no. 6, pp. 1755–1760, 1984.

[8] H. Seki, A. Granato, and R. Truell, "Diffraction effects in the ultrasonic field of a piston source and their importance in the accurate measurement of attenuation," *The Journal of The Acoustical Society of America*, vol. 28, pp. 230–238, March 1955.

[9] G. C. Benson and O. Kiyohara, "Tabulation of some integral functions describing diffraction effects in the ultrasonic field of a circular piston source," *J. Acoust. Soc. Am.*, vol. 55, pp. 184–185, January 1974.

[10] A. S. Khimunin, "Numerical calculation of the diffraction corrections for the precise measurement of ultrasound absorption," *Acustica*, vol. 27, no. 4, pp. 173–181, 1972.

[11] P. H. Rogers and A. L. Van Buren, "An exact expression for the lommel diffraction correction integral," *Acoust. Soc. Am.*, vol. 55, pp. 724–728, April 1974.

[12] J. H. Cantrell, "Acoustic generation from fatigue-induced dislocation dipoles," *Philosophical Magazine A*, vol. 69, no. 2, pp. 315–326, 1994.

[13] J. H. Cantrell, "Substructural organization, dislocation plasticity and harmonic generation in cyclically stressed wavy slip metals," *Proc. R. Soc. Lond. A*, vol. 460, pp. 757–780, 2004.

[14] J. H. Cantrell and W. T. Yost, "Nonlinear ultrasonic characterization of fatigue microstructures," *International Journal of Fatigue*, vol. 23, pp. S487–S490, 2001.

[15] E. Burke, "Non-linear acoustical behavior in a nickel-base superalloy and higher order harmonic liquid capacitive detection," Master's thesis, University of Dayton, Dayton, OH, December 2003.

[16] H. D. Young and R. A. Freedman, *University Physics*. Addison-Wesley Publishing Co., inc., ninth ed., 1996.

[17] W. T. Yost and J. H. Cantrell, "Absolute ultrasonic displacement amplitude measurements with a submersible electrostatic acoustic transducer," *Rev. Sci. Instrum.*, vol. 63, pp. 4182–4188, September 1992.

[18] R. Truell, C. Elbaum, and B. B. Chick, *Ultrasonic Methods in Solid State Physics*. Academic Press, Inc., 1969.